Inorganic Chemistry

Article

pubs.acs.org/IC

Trinuclear Complexes and Coordination Polymers of Redox-Active Guanidino-Functionalized Aromatic (GFA) Compounds with a Triphenylene Core

Anna Lebkücher, Christoph Wagner, Olaf Hübner, Elisabeth Kaifer, and Hans-Jörg Himmel*

Anorganisch-Chemisches Institut, Ruprecht-Karls Universität Heidelberg, Im Neuenheimer Feld 270, 69120 Heidelberg, Germany

Supporting Information

ABSTRACT: Herein, we report on the synthesis, redox activity, and coordination chemistry of 2,3,6,7,10,11-hexakis-(tetramethylguanidino)triphenylene. CV measurements indicated that the new compound could be oxidized in three separate reversible two-electron oxidation events. The HOMO and LUMO energies were estimated from the oxidation wave and the onset of absorption in the UV/vis spectrum. Our discussion also includes the related new compound 2,3,6,7,10,11-hexakis(*N*,*N*′-dimethylethyleneguanidino)triphenylene. Then trinuclear Cu^{I} and Cu^{II} complexes of the new triphenylene ligands were characterized, and their electronic properties are discussed. In contrast to previously studied redox-active GFA ligands, oxidation of trinuclear copper(I) iodide complexes with I_2 leads to copper instead of ligand oxidation. In the tetra-coordinated Cu^{II} complexes, the coordination mode is intermediate between tetrahedral and square planar. The optical properties of the complexes were studied, and low-energy electronic transitions were assigned to ligand-to-metal charge-transfer (LMCT) excitations. We then extended our analysis to trinuclear Ni^{II} and Co^{II} complexes. The magnetic coupling mediated through the triphenylene ligand in the trinuclear Cu^{II} and Co^{II} complexes was studied by SQUID magnetometry, revealing ferromagnetic coupling of the spin centers and different degrees of spin delocalization into the guanidino groups. Finally, we show that the GFA ligands could be linked to one- or two-dimensional coordination polymers and porous materials with a layer structure by reaction with silver halides.

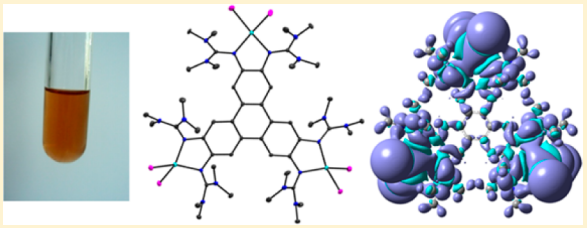

INTRODUCTION

Triphenylenes are used for a variety of purposes. They are applied as components in organic light-emitting diode (OLED) devices[1,2] and transistors,[3] and substitution allows control of their electronic properties.[2] A columnar phase of 2,3,6,7,10,11-hexakis(hexylthio)triphenylene was shown to be suitable for the fast transport of photogenerated charge carriers.[4] Moreover, ligands with triphenylene backbones have been studied. Very recently, a tris-carbene ligand with a triphenylene backbone was synthesized, and its trinuclear metal complexes were applied as catalysts in coupling reactions.[5] 2,3,6,7,10,11-Hexakis(arylthio)-triphenylenes (see Scheme 1) and 2,3,6,7,10,11-hexakis-(phenylseleno)triphenylene were connected by silver(I) to three-dimensional coordination networks.[6,7] Because of their rigidity, triphenylenes have also been employed for the synthesis of porous materials with layer structures.[8]

Guanidines are versatile ligands and substituents.[9] Bicyclic guanidinates have been used extensively for the stabilization of dinuclear transition-metal complexes with multiple bonds between two highly oxidized metal atoms[10] and for catalytic applications.[9g,11] Acyclic guanidinates with sterically demanding organic groups have been used as substituents in dimeric Mg^{I} compounds.[12] Neutral hybrid guanidine ligands have been applied in catalytic reactions such as lactide polymerization.[13] Moreover, the first structurally characterized end-on-bonded copper superoxo complex featured a tripodal guanidine ligand.[14] Guanidino-functionalized aromatic (GFA-*n*) compounds (where $n \geq 4$ denotes the number of guanidino groups) were established by us as a new class of redox-active

Scheme 1. Lewis Structure of 2,3,6,7,10,11-Hexakis(arylthio)triphenylenes Used for the Construction of Coordination Polymers

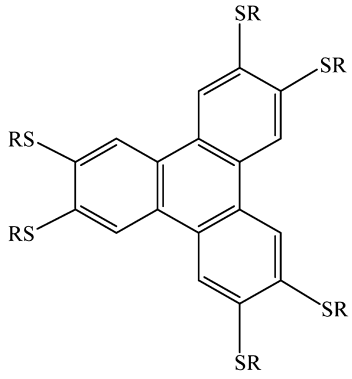

R = C_6H_5 or C_6H_4-*p*-OCH_3

Received: June 20, 2014
Published: September 4, 2014

   dx.doi.org/10.1021/ic501482u | *Inorg. Chem.* 2014, 53, 9876−9896

ligands,[15] with 1,2,4,5-tetrakis(tetramethylguanidino)benzene (**1**, see Scheme 2) being the first example.[16] In the case of dinuclear copper complexes, an almost-complete electron-transfer series was synthesized. In dinuclear Cu^{I} and Cu^{II} complexes, the redox-active ligand **1** could be either neutral or oxidized to a radical monocation or dication.[17,18] In some cases, oxidation of the ligand is accompanied by polymerization to give semiconducting coordination polymers.[19,20] Hence, oxidation of $\mathbf{1}(CuI)_2$ with I_2 leads to the chain polymer $\{[\mathbf{1}(CuI)_2](I_3)_2\}_n$.[19] In paramagnetic dinuclear Cu^{II}, Ni^{II}, or Co^{II} complexes, weak antiferromagnetic coupling mediated by the GFA ligand leads to a singlet ground state if the ligand is neutral or dicationic. On the other hand, a strong ferromagnetic coupling (between metal and ligand) and a high-spin ground state occurs if the ligand is oxidized to the radical monocation.[18] GFA compounds are not only interesting for applications in the area of coordination chemistry, but could also serve in C—H deprotonation[21] or photoinduced reductive coupling reactions.[22] Wrapped in a weakly bound dicationic complex, they can be used for the stabilization of extended polyanionic networks.[23,24] Several methods for varying the electron-donor capacity have been reported. In particular, aromatic substitution has a great influence on the energies and shapes of the frontier orbitals.[25] Modifications of the size of the aromatic system and the guanidino-substiution pattern are further possibilities for controlling the redox activity. For example, 1,4,5,8-tetrakis(tetramehylguanidino)naphthalene, **2** (see Scheme 2), has been shown to be a weaker electron donor than **1**.[26]

Herein, we report on the synthesis, redox behavior and coordination chemistry of 2,3,6,7,10,11-hexakis-(tetramethylguanidino)triphenylene, **3**. We also synthesized the related compound 2,3,6,7,10,11-hexakis-(dimethylethyleneguanidino)triphenylene, **4** (see Scheme 2). The guanidino groups perform four roles that are relevant for potential applications: (i) They shift the highest occupied molecular orbital (HOMO) of the triphenylene to higher energies, increasing the electron-donor capacity of the aromatic compound. (ii) They increase the solubility. (iii) They provide sites for metal coordination, leading to either trinuclear complexes or coordination polymers. (iv) They prevent aggregation through π-stacking. In previous works, 1,4,5,8,9,12-hexaazatriphenylene (HAT) was used as redox-active ligand and also an n-conducting material.[27−31] This compound is an electron acceptor [the N atoms lower the

Scheme 2. Known GFA-4 Compounds 1 and 2 and New GFA-6 Compounds 3 and 4

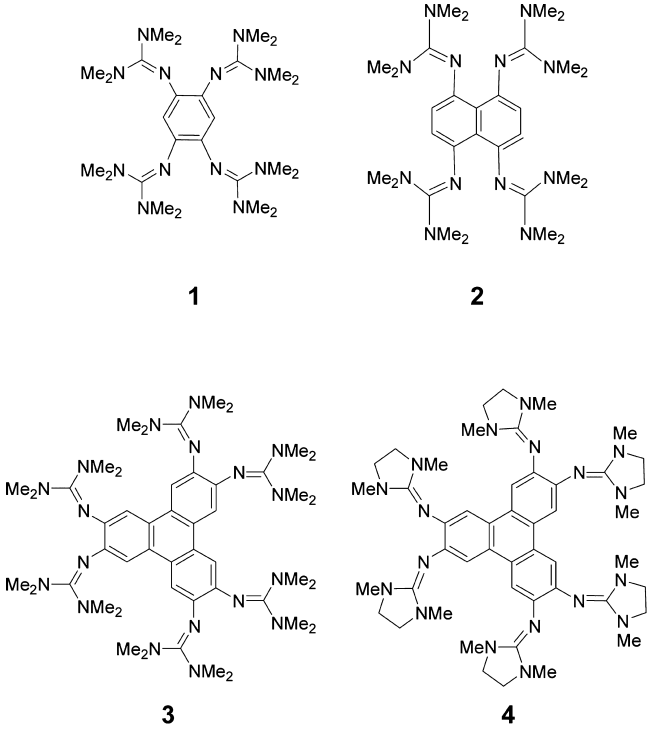

Scheme 3. Synthesis of the New Redox-Active Triphenylene Derivative 3

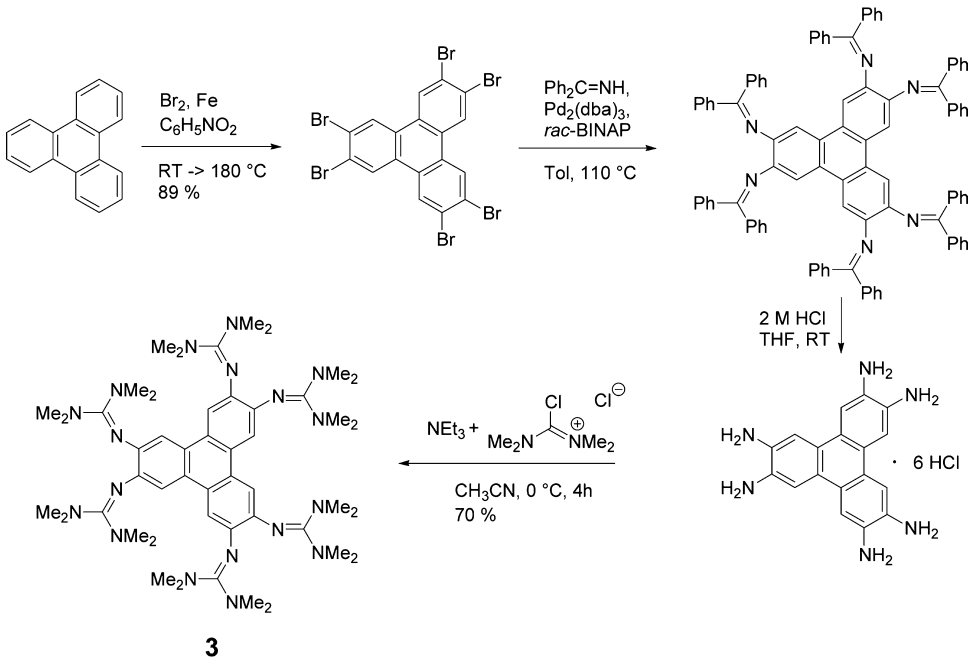

dx.doi.org/10.1021/ic501482u | Inorg. Chem. 2014, 53, 9876−9896

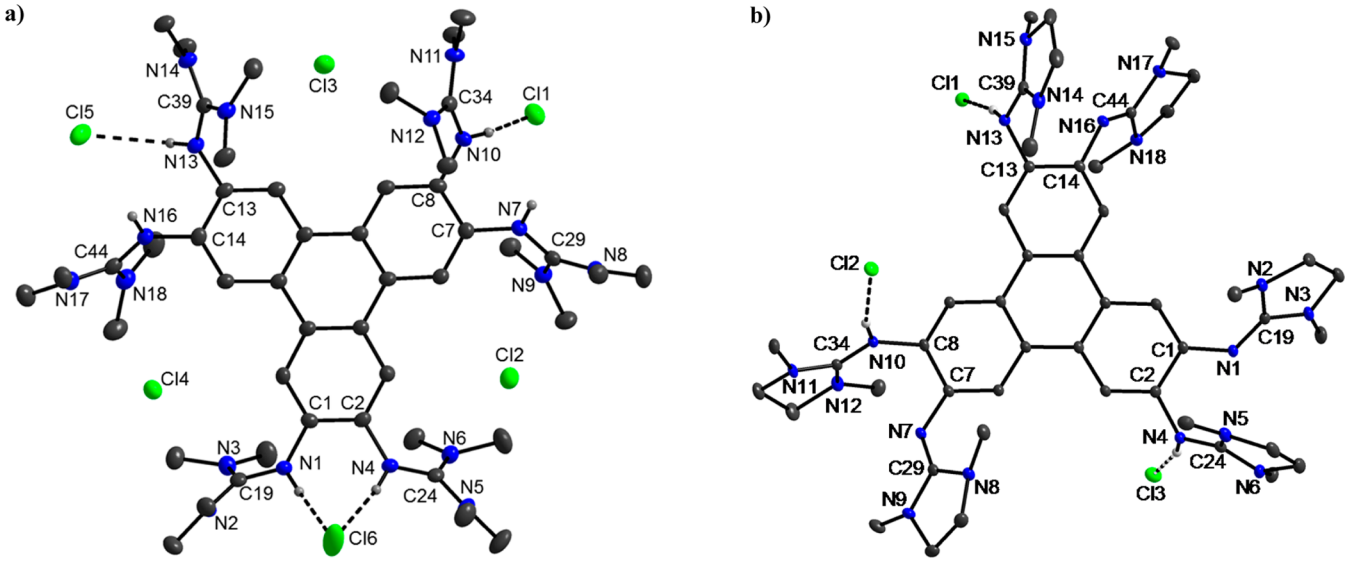

Figure 1. (a) Fraction of the structure of $[\mathbf{3}H_6]Cl_6$. Vibrational ellipsoids drawn at the 50% probability level. Hydrogen atoms omitted for the sake of clarity. Selected bond distances (in pm) and angles (in deg): N1—C1 1.425(3), N1—C19 1.358(3), N2—C19 1.334(3), N3—C19 1.333(3), N4—C24 1.353(3), N5—C24 1.339(3), N6—C24 1.331(3), N7—C7 1.415(3), N7—C29 1.355(3), N8—C29 1.334(3), N9—C29 1.334(3), N10—C8 1.420(3), N10—C34 1.348(3), N11—C34 1.330(3), N12—C34 1.342(3), N13—C13 1.422(2), N13—C39 1.350(3), N14—C39 1.337(3), N15—C39 1.331(3), N16—C14 1.423(3), N16—C44 1.359(3), N17—C44 1.327(3), N18—C44 1.339(3), C1—C2 1.411(3), C7—C8 1.409(3), C13—C14 1.403(3), C1—N1—C19 126.78(17), C2—N4—C24 126.12(17), C7—N7—C29 126.25(17), C8—N10—C34 121.74(17), C13—N13—C39 126.85(17), C14—N16—C44 124.51(17). (b) Fraction of the structure of $[\mathbf{4}H_3]Cl_3$. Vibrational ellipsoids drawn at the 50% probability level. Hydrogen atoms omitted for the sake of clarity. Selected bond distances (in pm) and angles (in deg): N1—C1 1.389(2), N1—C19 1.311(2), N2—C19 1.370(2), N3—C19 1.354(2), N4—C2 1.434(2), N4—C24 1.343(2), N5—C24 1.331(2), N6—C24 1.343(2), N7—C7 1.393(2), N7—C29 1.292(2), N8—C29 1.393(2), N9—C29 1.365(2), N10—C8 1.429(2), N10—C34 1.329(2), N11—C34 1.339(2), N12—C34 1.340(2), N13—C13 1.441(2), N13—C39 1.337(2), N14—C39 1.338(2), N15—C39 1.341(2), N16—C14 1.394(2), N16—C44 1.300(2), N17—C44 1.367(2), N18—C44 1.383(2), C1—C2 1.416(2), C7—C8 1.420(2), C13—C14 1.407(2), C1—N1—C19 124.31(15), C2—N4—C24 119.59(15), C7—N7—C29 124.29(15), C8—N10—C34 127.32(15), C13—N13—C39 117.30(14), C14—N16—C44 120.96(14).

energies of the lowest unoccupied molecular orbital (LUMO) and HOMO with respect to those of triphenylene]. By contrast, we will show herein that **3** and **4** are quite strong electron donors.

RESULTS AND DISCUSSION

Synthesis and Characterization of 3 and 4. Starting with 2,3,6,7,10,11-hexabromotriphenylene, which was prepared according to the literature method,[32] the hexamine derivative was synthesized in a two-step reaction.[33] The hexamine was then converted to the hexaguanidines **3** and **4** by reaction with the "activated ureas" or "Vilsmeier" salts 2-chloro-1,1,3,3-tetramethylformamidinium chloride and 2-chloro-1,3-dimethylimidazolinium chloride, respectively (see Scheme 3 for the synthesis of **3**). The new compounds are pale-yellow-colored solids that must be stored under inert-gas atmosphere to avoid protonation or slow oxidation by O_2. The crystals of the compounds were unfortunately of poor quality, but nevertheless, the structure of **4** was measured (see Figure S1 in the Supporting Information) and confirmed the absence of π-stacking between the triphenylene cores in the solid state as a result of the steric demand of the guanidino groups. In addition, it was possible to obtain good-quality single crystals suitable for X-ray diffraction for the hexa-protonated species **3**·6HCl and for the tris-protonated species **4**·3HCl. Both compounds were prepared by reaction of the bases **3** and **4** with 6 equiv of HCl. The observation that **4** binds only three protons whereas **3** binds six can be rationalized by the reduced basicity of the *N,N′*-dimethylethyleneguanidino group compared with the tetramethylguanidino group.[34] The structures are illustrated in Figure 1. Protonation occurs exclusively at the imino N atoms and leads to an increase of the imino C═N bond distance (see the structural differences between protonated and unprotonated guanidino groups in **4**·3HCl). The triphenylene core remains planar. Below, it is shown that coordination can cause significant distortions of the triphenylene core.

The cyclic voltammetry (CV) curve of **3** (see Figure 2a) shows three reversible redox processes, which we assign to two-electron redox events (on the basis of the intensities relative to that of ferrocene as well as comparison with other GFAs). The curve obtained for **1** is also included for comparison. The presence of a one-electron wave at higher potential ($E_{1/2}$ = 0.68 V) in the curve of **1** is in line with the conversion of two electrons in the wave at lower potential ($E_{1/2}$ = −0.76 V). A CV curve of a 1:2 mixture of compound **1** and ferrocene is shown in Figure S2a of the Supporting Information. The second reduction wave in the CV curve of **3** has a doublet structure indicating that reduction from $\mathbf{3}^{4+}$ to $\mathbf{3}^{2+}$ occurs in two unresolved one-electron steps. This behavior proved to be independent of the scan rate (see the curves for different scan rates in Figure S2b of the Supporting Information). The CV curve of **4** looks similar, but the waves show larger shoulders (see Figure S3 in the Supporting Information). Table 1 summarizes the potentials measured for **3**. The $E_{1/2}$ value of the first two-electron redox event is −0.39 V vs $Fc^{+/0}$. This value compares with −0.76 V (also vs $Fc^{+/0}$) determined for **1**. The $E_{1/2}$ value for the redox couple $\mathbf{4}^{+2/0}$, as measured by CV in CH_2Cl_2 solution, is slightly more negative (−0.40 V vs $Fc^{+/0}$; see the CV curve in the Supporting Information). The same trend was observed upon changing the guanidino groups in

dx.doi.org/10.1021/ic501482u | Inorg. Chem. 2014, 53, 9876−9896

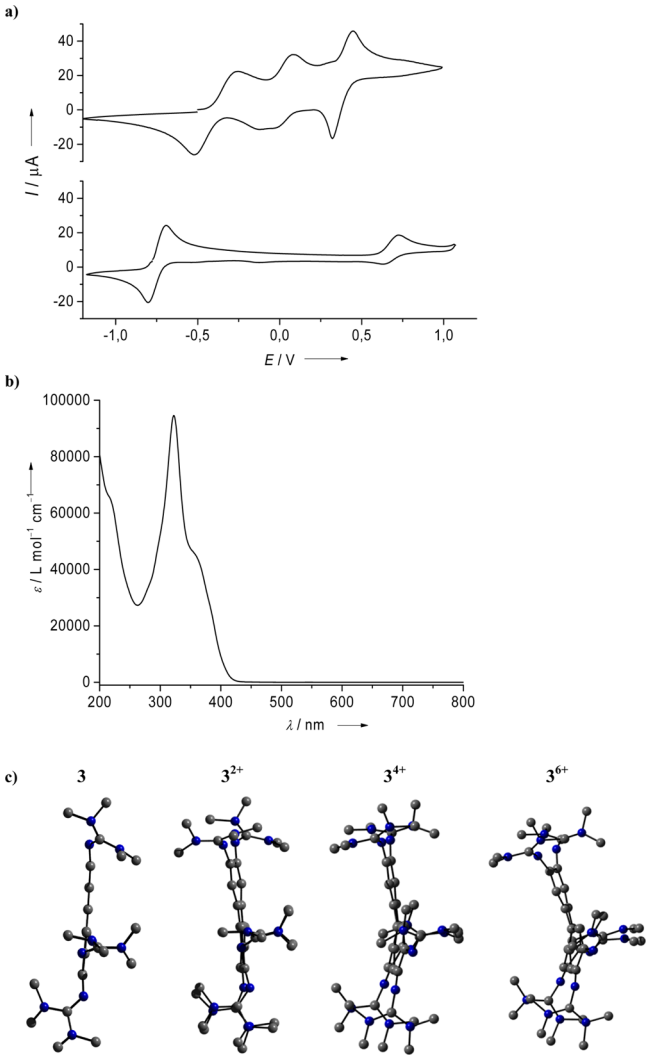

Figure 2. (a) CV curve of **3** (potential vs $Fc^{+/0}$, CH_2Cl_2 solution, with $[n\text{-}Bu_4N][PF_6]$ as the supporting electrolyte, scan speed of 100 mV s^{-1}). The curve recorded for **1** is included for comparison. (b) UV/vis spectrum of **3** in CH_3CN. (c) Comparison between the structures calculated for **3**, 3^{2+}, 3^{4+}, and 3^{6+} (B3LYP/6-311G** calculations).

Table 1. Results of the CV Measurements for 3 and 4 in CH_2Cl_2 Solution[a]

	E_{ox} (V)	E_{red} (V)	$E_{1/2}$ (V)
	Compound **3**		
first two-e^- wave	−0.25	−0.52	−0.39
second two-e^- wave	0.08	−0.12	0.02
third two-e^- wave	0.45	0.32	0.38
	Compound **4**		
first two-e^- wave	−0.32	−0.49	−0.40
second two-e^- wave	0.02	−0.09	0.03
third two-e^- wave	0.51	0.36	0.43

[a]All potentials given relative to the redox couple $Fc^{+/0}$ (Ag/AgCl electrode, $[n\text{Bu}_4\text{N}][PF_6]$ as the conducting salt).

compound **1**.[34] The difference between E_{ox} and E_{red} for the first two-electron redox event of each **3** and **4** is relatively large, which might argue for significant structural differences between the neutral and dicationic species. For the second and third two-electron redox events of **3** and **4**, $E_{1/2}$ values of 0.02 and 0.38 V vs $Fc^{+/0}$, respectively, for **3** and 0.03 and 0.43 V vs $Fc^{+/0}$, respectively, for **4** were measured.

The CV measurements highlight the difference between the redox-active guanidino-functionalized triphenylenes **3** and **4** and the previously reported, also redox-active, HAT (1,4,5,8,9,12-hexaazatriphenylene) ligand.[27−31] Whereas **3** and **4** are quite strong organic electron donors, HAT is an electron acceptor. Figure S4 in the Supporting Information illustrates the changes in the HOMO energy and the HOMO−LUMO gap upon substitution of triphenylene with four guanidino groups calculated at the B3LYP/6-311G** level. Using a simple relationship,[35] the HOMO energy of **3** can be estimated from the oxidation potential to be ca. −4.8 eV. Hence, as a direct consequence of the electron-donating guanidino groups, the HOMO energy is high in comparison with those of typical triphenylene derivatives used in OLED devices.[2] On the other hand, it is lower than that of **1** (ca. −4.4 eV). The UV/vis spectrum (see Figure 2b) provides evidence for a very strong electronic transition centered at 322 nm and weaker electronic transitions at 356 nm (shoulder) and ca. 215 nm. From the onset in the absorption spectrum at ca. 420 nm (3 eV), the LUMO energy can be estimated to be around −1.8 eV. Compound **3** can be evaporated without decomposition at a temperature of ca. 450 °C in a vacuum (3×10^{-2} mbar).

Various oxidation agents, such as iodine, bromine, tetracyanoquinodimethane (TCNQ), and $AgPF_6$, were tested to chemically oxidize compounds **3** and **4**, and distinct color changes from pale yellow to deep blue, purple, and green, respectively, indeed signaled reactions leading to the breakup of the aromatic system. However, product mixtures were formed, and the oxidized species turned out to be highly unstable, so that all attempts thus far to isolate a pure species failed. Therefore, the structures and energies of **3**, 3^{2+}, 3^{4+}, and 3^{6+} were calculated using density functional theory (DFT) methods (B3LYP functional in combination with the 6-311G** basis set). The calculated minimum structures are sketched in Figure 2c, and Table 2 provides selected bond distances (as defined in Scheme 4). It can be seen that the triphenylene core loses its planarity upon oxidation and becomes increasingly folded with increasing electron release. The most oxidized species, 3^{6+}, is a radialene derivative. Radialene itself is extremely unstable, and only a few derivatives have been structurally characterized.[36] With increasing charge, the bond distances indeed increasingly adopt the values expected for the radialene structure. Hence, the lengths of bonds a, b, d, and g increase, whereas the length of bond c decreases. Bond e, which is a C—N single bond in neutral **3**, decreases in length to a value typical for a C═N double bond. In contrast, bond f (the imino N═C double bond in neutral **3**) increases in length to a value typical for a single bond.

The Gibbs free energy for the gas-phase electron-transfer reaction between **1** and 3^{2+} (see Scheme 5) was calculated to be only −1 kJ mol^{-1}, a result that at first glance argues for a similar electron-donor capacity. On the other hand, the CV data clearly show **3** to be a weaker electron donor than **1** in CH_2Cl_2 solution. In 3^{2+}, the positive charge is delocalized over a large number of atoms. The seeming discrepancy can therefore be explained by the poorer solvent stabilization of the dication 3^{2+} in comparison to 1^{2+}. The large solvent influence on redox reactions with **1** was already discussed by us previously.[16] According to our calculations, a hypothetical electron-transfer reaction in the gas phase between 1,2-bis-(tetramethylguanidino)benzene and 3^{2+} (see the second

dx.doi.org/10.1021/ic501482u | Inorg. Chem. 2014, 53, 9876−9896

Table 2. Selected Bond Distances (in Å) as Obtained from DFT Calculations (B3LYP/6-311G**) for Neutral and Oxidized 3[a]

bond	3	3^{2+}	3^{4+}	3^{6+}
a	1.421−1.428	1.429−1.485	1.500−1.502	1.525−1.527
b	1.387−1.391	1.378−1.429	1.427−1.430	1.463−1.465
c	1.409−1.411	1.375−1.426	1.381−1.383	1.362−1.364
d	1.418	1.411−1.471	1.462−1.468	1.484−1.493
e	1.394−1.403	1.307−1.381	1.297−1.304	1.275−1.277
f	1.285−1.286	1.297−1.343	1.352−1.356	1.385−1.388
g	1.463	1.415−1.468	1.455−1.457	1.482−1.488

[a]See Scheme 4 for bond notation.

Scheme 4. Definitions of Some Bond Distances Used in Table 2 and Lewis Structure of the Species with the Highest Possible Charge, 3^{6+}

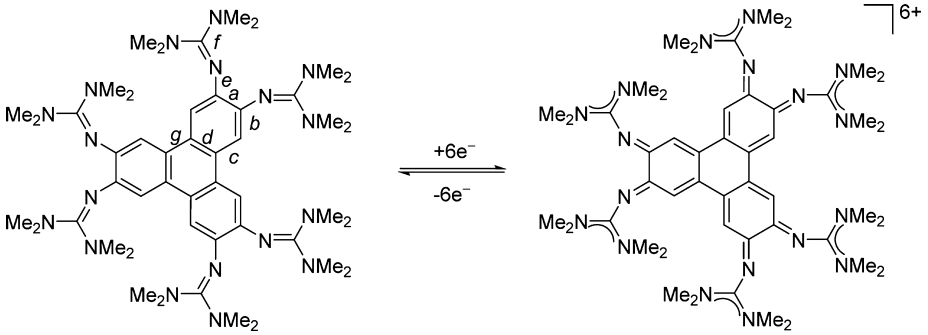

Scheme 5. Calculated Gas-Phase Redox Reactions to Compare 3 in Its "Intrinsic" Electron-Donor Capacity with Other Guanidino-Functionalized Aromatic Compounds

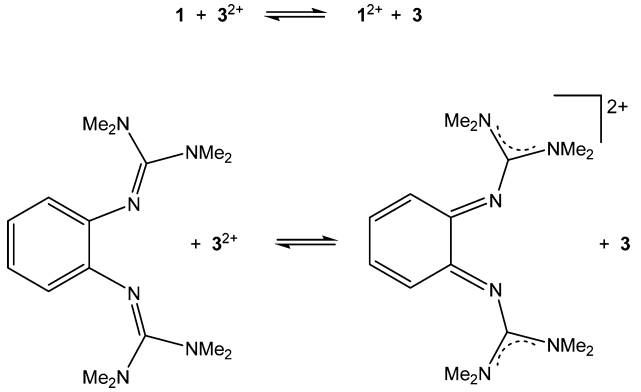

reaction in Scheme 5) is highly endergonic [ΔG = +278 kJ mol^{-1} at standard conditions (1 bar, 298 K)]. Hence, compound **3** cannot be described simply as three (*o*-bisguanidino)benzene units fused together by C—C single bonds.

Coordination Chemistry. Reaction of **3** with CuX (X = CN, Cl, Br, or I) yielded the trinuclear complexes **3**$(CuX)_3$. The highest yield was obtained for X = CN (almost 90%), and the lowest for X = I (ca. 60%). The complexes **3**$(CuCN)_3$, **3**$(CuCl)_3$, and **3**$(CuBr)_3$ were structurally characterized by single-crystal X-ray diffraction. Their structures are illustrated in Figures 3 and 4. In all cases, coordination was accompanied by a quite large distortion of the triphenylene core, leading to the loss of planarity of the central C_6 ring (see Figure 3b). All Cu—N bonds are very similar in length and adopt average values of 2.021 Å in **3**$(CuCN)_3$, 2.033 Å in **3**$(CuCl)_3$, and 2.024 Å in **3**$(CuBr)_3$. In previous work, the metal−guanidine bonding in GFA complexes was analyzed, and it was found that the bond consists of both σ- and π-contributions.[37] Consequently, the imino bond length significantly increases upon coordination. In **3**$(CuCN)_3$, **3**$(CuCl)_3$, and **3**$(CuBr)_3$, average N═C bond distances of 1.326, 1.323, and 1.330 Å, respectively, were found.

The electronic absorption spectra were found to be similar for all four Cu^I compounds. Figure 4c shows as example the spectrum of **3**$(CuI)_3$ [that of **3**$(CuCN)_3$ is included in Figure S5 of the Supporting Information]. Four strong absorptions were detected above 300 nm, centered at 313, 342, 380, and 399 nm. For comparison, in the case of **3**, only two absorptions above 300 nm, with maxima at 322 and 356 nm, were found. The experimentally obtained spectrum was compared with a simulation based on time-dependent density functional theory (TD-DFT) calculations (see Figure 4c). We used the B3LYP method, which was previously shown to provide reasonable results for guanidine−copper complexes (see the details of the quantum chemical calculations at the end of this work for more information).[38] The bands labeled 1, 2, and 3 (see Figure 4c) all belong to transitions with a dominant degree of charge transfer from the CuI units to the guanidine ligand **3**, and in all cases, the LUMO and LUMO + 1 (both located on the guanidine ligand) are involved (see the orbital pictures in Figure 4d and Figures S6 and S7 and Table S1 in the Supporting Information for more details). The shoulder at 399 nm in the measured spectrum was assigned to two transitions calculated to appear at 432 nm (labeled 1), in which the excitations from the HOMO − 2 (located on the Cu and I orbitals) into the LUMO and LUMO + 1 predominantly participate.

The Cu^I complexes appear to be generally quite unstable in solutions of organohalides. When **3**$(CuI)_3$ was dissolved in a $CHCl_3/Et_2O$ mixture, green-colored crystals of **3**$(CuCl_2)_3$ formed after some time. However, this reaction is slow and therefore (at least under the chosen conditions) not suitable for the synthesis of **3**$(CuCl_2)_3$ in larger quantities.

dx.doi.org/10.1021/ic501482u | Inorg. Chem. 2014, 53, 9876−9896

a)

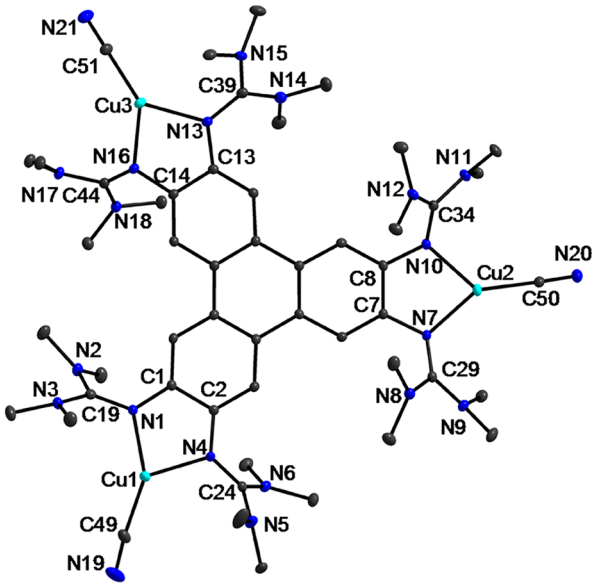

b)

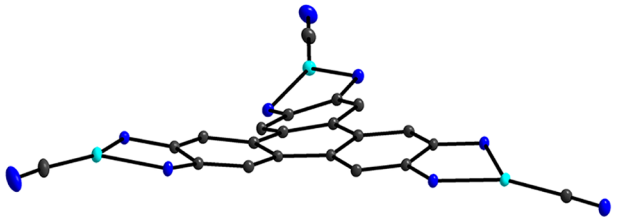

Figure 3. (a) Molecular structure of the trinuclear complex $3(CuCN)_3$. Vibrational ellipsoids drawn at the 50% probability level. Hydrogen atoms omitted for the sake of clarity. Selected bond distances (in Å) and angles (in deg): Cu1—N1 1.998(3), Cu1—N4 2.034(3), Cu1—C49 1.862(4), Cu2—N7 2.005(3), Cu2—N10 2.038(3), Cu2—C50 1.860(3), Cu3—N13 2.046(3), Cu3—N16 2.007(3), Cu3—C51 1.867(3), N1—C1 1.405(4), N1—C19 1.329(4), N2—C19 1.366(4), N3—C19 1.353(4), N4—C2 1.405(4), N4—C24 1.327(4), N5—C24 1.358(4), N6—C24 1.351(4), N7—C29 1.320(4), N8—C29 1.377(4), N9—C29 1.362(4), N10—C34 1.330(4), N11—C34 1.361(4), N12—C34 1.354(4), N13—C13 1.409(4), N13—C39 1.327(4), N14—C39 1.362(4), N15—C39 1.363(4), N16—C14 1.406(4), N16—C44 1.324(4), N17—C44 1.357(4), N18—C44 1.372(4), C1—C2 1.427(4), C7—C8 1.422(4), C13—C14 1.415(4), N1—Cu1—N4 82.18(11), N1—Cu1—C49 150.69(14), N4—Cu1—C49 126.34(14), Cu1—C49—N19 173.7(4), N7—Cu2—N10 82.74(10), N7—Cu2—C50 145.78(12), N10—Cu2—C50 131.43(13), Cu2—C50—N20 176.8(3), N13—Cu3—N16 81.94(11), N13—Cu3—C51 135.91(14), N16—Cu3—C51 142.15(14), Cu3—C51—N21 177.1(4). (b) View from a different perspective showing the curled structure of the triphenyl system.

Trinuclear Cu^{II} complexes of ligand **3** could be synthesized in two different ways. The first is direct reaction between a copper(II) halide and **3**. Hence, ligand **3** was found to react with 3 equiv of $CuCl_2$ or $CuBr_2$ to give the complexes $3(CuCl_2)_3$ or $3(CuBr_2)_3$, respectively. Such a reaction is generally not possible in the case of compound **1**, as it leads to oxidation of the guanidine ligand and formation of dinuclear Cu^{II} complexes of the guanidine dication. Only in exceptional cases was the isolation of dinuclear Cu^{II} complexes of neutral **1** possible, for example, the complex $1\{(Cu(NO_3)_2\}_2$.[18] The second, more interesting approach, is oxidation of a trinuclear Cu^{I} complex of **3** (see Scheme 6). Hence, oxidation of $3(CuI)_3$ with I_2 resulted in copper oxidation to give $3(CuI_2)_3$. This reaction is remarkable in several ways. First, Cu^{II} is unstable in the presence of iodide in aqueous solution.[39] On the other hand, in nonaqueous solutions, some Cu^{II} complexes with iodide ligands have been reported, such as with pyridine ligands, an example being $[Cu(py)_4I]I{\cdot}2py$,[40] or with β-diketiminate ligands.[41] However, the complex $3(CuI_2)_3$ is unique in that each copper is coordinated to two iodides with similar Cu—I distances (see discussion of the structure below). The reactivity of $3(CuI)_3$ toward I_2 is in sharp contrast to that observed for previously studied Cu^{I} complexes of redox-active GFA ligands. Hence, reaction of $1(CuI)_2$ with I_2 leads exclusively to ligand instead of copper oxidation, yielding the semiconducting coordination polymer $\{[1(CuI)_2](I_3)_2\}_n$.[19] According to quantum chemical calculations [B3LYP/def2-SV(P)], the gas-phase ΔG value (at standard conditions) for oxidation of $3(CuI)_3$ with I_2 to give $3(CuI_2)_3$ (second equation in Scheme 6) amounts to only -20 kJ mol^{-1}. In solution, $3(CuI_2)_3$ shows no sign of I_2 elimination. The complex decomposes slowly in $CHCl_3$ at 65 °C to unknown products. We noticed that, in CH_2Cl_2 solution, the iodide is slowly exchanged by chloride. The thermogravimetry (TG) curve (see Figure S8 in the Supporting Information) showed weight loss (presumably with elimination of I_2) in several steps at temperatures higher than 150 °C.

We achieved the structural characterization of $3(CuCl_2)_3$ and $3(CuI_2)_3$ by single-crystal X-ray diffraction. The structure of $3(CuCl_2)_3$ is displayed in Figure 5. The Cu—N distances (1.972 Å on average) are slightly shorter than those in $3(CuCl)_3$ (2.033 Å on average). A stronger ligand−metal interaction also manifests itself in the elongated C═N bond (1.344 Å on average). Whereas the triphenylene core is almost planar in the case of $3(CuCl_2)_3$, it is highly curled for $3(CuCl)_3$. A structural detail of importance for the understanding of the electronic absorption spectra and also the magnetic superexchange (see discussion below) is the dihedral angle between the Cl—Cu—Cl and N—Cu—N planes, which measures 44° (Cu1) and 50° (Cu2) and is therefore halfway between the value of 0° for square-planar coordination and 90° for tetrahedral coordination. According to theoretical analysis, Cu^{II} prefers a distorted trigonal coordination in the presence of π-donor ligands,[42] in agreement with recent experimental results.[43] The structure of $3(CuI_2)_3$ is shown in Figure S8 in the Supporting Information. It is similar to that of $3(CuCl_2)_3$. The average dihedral angle between the N—Cu—N and I—Cu—I planes measures 55°, thus being even closer to tetrahedral than to square-planar coordination. In line with the relatively low coordination number, the Cu—I distances are relatively short, measuring 2.559 Å on average. For comparison, for the complex $[Cu(py)_4I]I{\cdot}2py$, a Cu—I distance of 2.951(1) Å was reported.[40] On the other hand, in the β-diketiminate complex $(Me_2NN)CuI$ [Me_2NN = 2,4-bis(2,6-dimethylphenylimido)-pentyl], featuring three-coordinated Cu^{II} centers, a shorter Cu—I distance of 2.4295(5) Å was measured.[41] In contrast to the situation in the Cu^{I} complexes, the triphenylene core is planar in the Cu^{II} complex $3(CuI_2)_3$ [as in $3(CuCl_2)_3$].

The three Cu^{II} complexes $3(CuX_2)_3$ exhibit different optical properties, as evidenced by their colors in CH_2Cl_2 solution (see

dx.doi.org/10.1021/ic501482u | Inorg. Chem. 2014, 53, 9876−9896

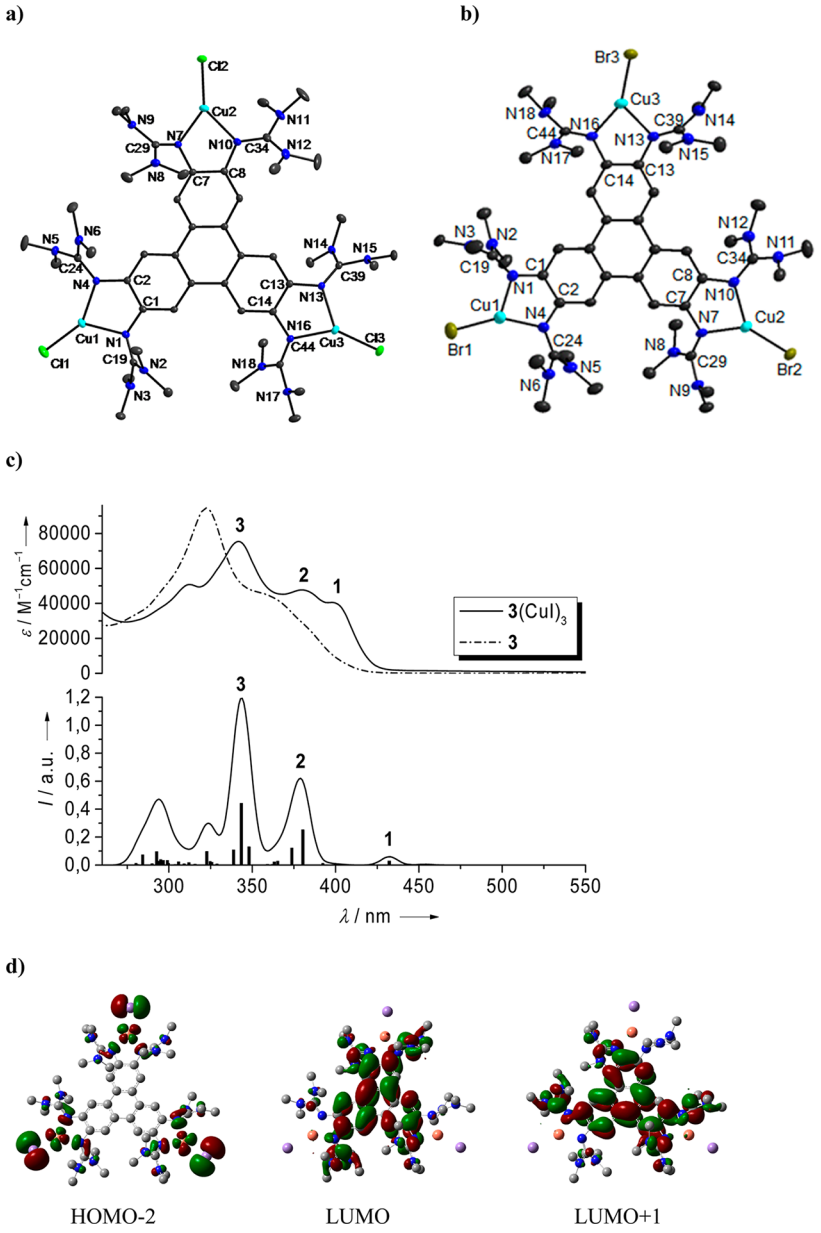

Figure 4. (a) Molecular structure of the trinuclear complex **3**$(CuCl)_3$. Vibrational ellipsoids drawn at the 50% probability level. Hydrogen atoms omitted for the sake of clarity. Selected bond distances (in Å) and angles (in deg): Cu1—Cl1 2.1480(11), Cu1—N1 2.038(3), Cu1—N4 2.013(3), Cu2—Cl2 2.1682(10), Cu2—N7 2.003(3), Cu2—N10 2.074(3), Cu3—Cl3 2.1478(10), Cu3—N13 2.047(3), Cu3—N16 2.022(3), N1—C1 1.401(4), N1—C19 1.324(4), N2—C19 1.363(4), N3—C19 1.359(4), N4—C24 1.325(4), N5—C24 1.359(4), N6—C24 1.364(5), N7—C7 1.406(4), N7—C29 1.334(4), N8—C29 1.355(4), N9—C29 1.356(4), N10—C8 1.407(4), N10—C34 1.317(5), N11—C34 1.380(6), N12—C34 1.354(6), N13—C13 1.401(4), N13—C39 1.325(4), N14—C39 1.356(4), N15—C39 1.364(4), N16—C44 1.314(4), N17—C44 1.369(4), N18—C44 1.378(5), C1—C2 1.431(4), C7—C8 1.419(4), C13—C14 1.418(4), N1—Cu1—N4 82.74(11), N7—Cu2—N10 82.18(11), N13—Cu3—N16 82.84(11). (b) Molecular structure of the trinuclear complex **3**$(CuBr)_3$. Hydrogen atoms omitted for the sake of clarity. Selected bond distances (in Å) and angles (in deg): Cu1—Br1 2.2701(10), Cu1—N1 2.020(5), Cu1—N4 2.005(4), Cu2—Br2 2.2945(12), Cu2—N7 2.009(4), Cu2—N10 2.041(4), Cu3—Br3 2.2728(16), Cu3—N13 2.069(4), Cu3—N16 1.998(4), N1—C1 1.402(6), N1—C19 1.336(6), N2—C19 1.366(7), N3—C19 1.354(7), N4—C2 1.409(6), N4—C24 1.318(7), N5—C24 1.369(7), N6—C24 1.354(7), N7—C7 1.405(6), N7—C29 1.335(7), N8—C29 1.354(7), N9—C29 1.363(6), N10—C8 1.402(6), N10—C34 1.331(7), N11—C34 1.351(6), N12—C34 1.370(7), C1—C2 1.427(7), C7—C8 1.434(7), C13—C14 1.420(7), N1—Cu1—N4 82.98(17), N1—Cu1—Br1 124.00(12), N4—Cu1—Br1 152.57(13), N7—Cu2—N10 82.62(16), N7—Cu2—Br2 140.63(12), N10—Cu2—Br2 136.69(12), N13—Cu3—N16 83.74(17), N13—Cu3—Br3 125.62(12), N16—Cu3—Br3 150.08(12). (c) Comparison between the experimental UV/vis spectrum of **3**$(CuI)_3$ and a simulation on the basis of time-dependent density functional theory (TD-DFT) calculations. (d) Visualization of the isodensity surfaces for some orbitals involved in the electronic transitions.

Figure 6a and Figure S9 in the Supporting Information). In Figure 6b, the UV/vis spectrum of **3**$(CuI_2)_3$ is compared to those of **3** and **3**$(CuI)_3$. A broad transition near 497 nm with an extinction coefficient of 8106 M^{-1} cm^{-1} and an even broader absorption at 911 nm with an extinction coefficient of 4281 M^{-1} cm^{-1} are present in the spectrum of **3**$(CuI_2)_3$, but not in the spectra of **3** and **3**$(CuI)_3$. The extinction coefficient at 911 nm was measured for several concentrations of **3**$(CuI_2)_3$ in

dx.doi.org/10.1021/ic501482u | Inorg. Chem. 2014, 53, 9876−9896

Scheme 6. Synthesis of Cu^{II} Complexes of 3 by Reaction with $CuCl_2$ or Oxidation of $3(CuI)_3$[a]

$$\mathbf{3} + CuX_2 \longrightarrow \mathbf{3}(CuX_2)_3 \quad (X = Cl, Br)$$

$$\mathbf{3}(CuI)_3 + 1.5\ I_2 \longrightarrow \mathbf{3}(CuI_2)_3$$

$$\mathbf{1}(CuI)_2 + 3\ I_2 \longrightarrow 1/n\ \{[\mathbf{1}(CuI)_2](I_3)_2\}_n$$

[a]The analogous reaction for $\mathbf{1}(CuI)_2$ led to ligand instead of copper oxidation and the formation of a chain polymer.

a)

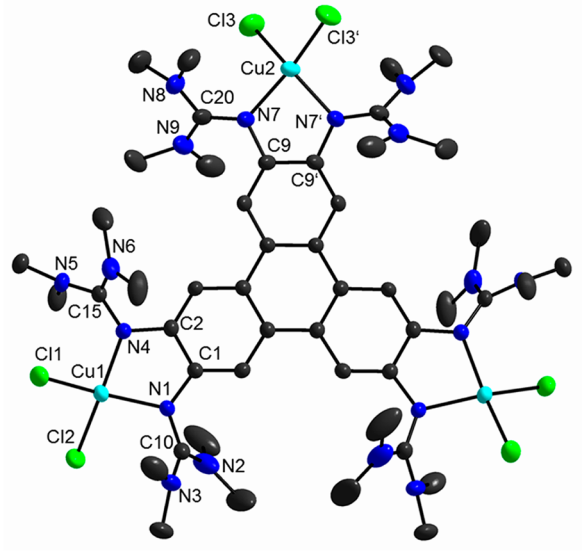

b)

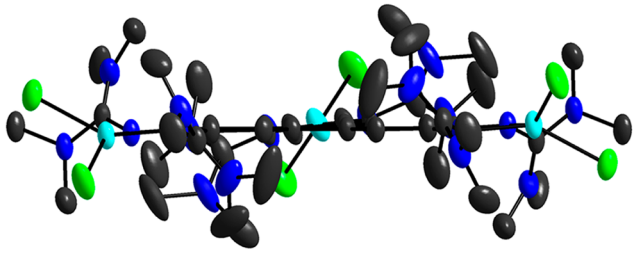

Figure 5. (a) Molecular structure of the trinuclear complex $3(CuCl_2)_3$. Vibrational ellipsoids drawn at the 50% probability level. Hydrogen atoms omitted for the sake of clarity. Selected bond distances (in Å) and angles (in deg): Cu1—Cl1 2.2465(11), Cu1—Cl2 2.2372(11), Cu1—N1 1.983(3), Cu1—N4 1.958(3), Cu2—Cl3 2.2401(12), Cu2—N7 1.974(3), N1—C1 1.406(4), N1—C10 1.340(4), N2—C10 1.322(5), N3—C10 1.345(5), N4—C2 1.399(4), N4—C15 1.357(4), N5—C15 1.342(4), N6—C15 1.332(5), N7—C9 1.414(4), N7—C20 1.336(5), N8—C20 1.340(6), N9—C20 1.350(6), C1—C2 1.420(4), C9—C9′ 1.404(7), Cl1—Cu1—Cl2 98.51(4), N1—Cu1—N4 82.72(11), Cl3—Cu2—Cl3′ 100.09(8), N7—Cu2—N7′ 83.55(17). (b) View from a different perspective showing the coordination mode of the copper ions.

CH_2Cl_2, and a plot of the extinction coefficient as a function of concentration confirms a linear relationship in accordance with the Lambert–Beer law (see Figure S10 in the Supporting Information). Interestingly, this band shifts considerably toward lower energy from $3(CuCl_2)_3$ (688 nm, ε = 1486 M^{-1} cm^{-1}) to

a)

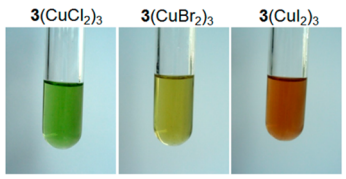

b)

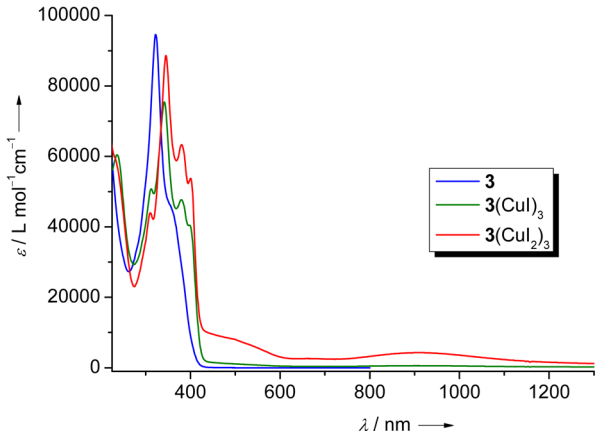

Figure 6. (a) Photographs showing the different colors of the trinuclear Cu^{II} complexes $3(CuCl_2)_3$, $3(CuBr_2)_3$, and $3(CuI_2)_3$. (b) Comparison of the UV/vis spectra of **3**, $3(CuI)_3$, and $3(CuI_2)_3$ in CH_2Cl_2 solution.

$3(CuBr_2)_3$ (754 nm, ε = 2132 M^{-1} cm^{-1}) and again to $3(CuI_2)_3$ (911 nm, ε = 4281 M^{-1} cm^{-1}). At the same time, the extinction coefficient of the band increases. TD-DFT calculations were performed for $3(CuI_2)_3$ to allow a better understanding of these lower-energy electronic transitions. In Figure 7a, the absorption spectrum in CH_2Cl_2 is compared with the calculated transitions (see Figures S11 and S12 and Tables S2 and S3 in the Supporting Information for more details). All calculated transitions above 420 nm involve predominantly the three unoccupied spin orbitals of lowest energy (365β, 366β, and 366α) as acceptor orbitals (see Figure 7b). These three orbitals are located on the CuI units. The excitation from spin orbital 365α into spin orbital 368α, both of which are located at ligand **3**, participates most in the transition at 391 nm, and therefore, this transition can be described as π–π^* excitation. The transitions within the range 420–1500 nm exhibit dominant ligand-to-metal charge-transfer (LMCT) character. Strong transitions were predicted in the range 500–700 nm, and these were assigned to the broad band near 500 nm in the experimental spectrum. This band is absent in the spectrum of $3(CuI)_3$. Two transitions with relatively high oscillator strength were calculated to appear at 1384 nm. We tentatively assign these two LMCT transitions to the broad band centered at 911 nm in the experimental UV/vis spectrum, although the level of agreement is quite poor. In principal, the band could also arise from a d–d transition. However, according to the TD-DFT calculations, the d–d transitions of $3(CuI_2)_3$ are much weaker and exhibit much lower energies (1975–1980 nm).

We also studied the redox properties of the complexes by cyclic voltammetry (CV). Although the CV curves (see Figure S13 in the Supporting Information) show several features that are difficult to explain, the major waves can be assigned to

dx.doi.org/10.1021/ic501482u | Inorg. Chem. 2014, 53, 9876–9896

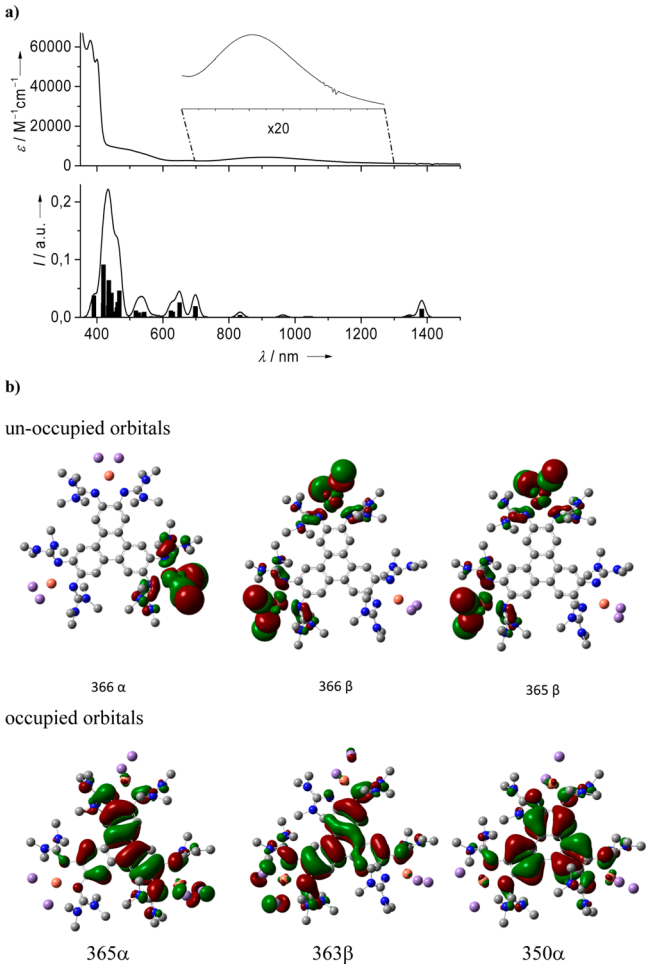

Figure 7. (a) Comparison between the absorption spectrum of $3(CuI_2)_3$ in CH_2Cl_2 and the transitions calculated by TD-DFT [B3LYP/def2-SV(P)]. (b) Isodensity surfaces of unoccupied (top) and occupied (bottom) spin orbitals involved in the electronic transitions.

metal- or ligand-centered redox processes. In the case of $3(CuCl_2)_3$, on sweeping to lower potentials, reduction of the Cu^{II} ions to Cu^{I} gives rise to a broad wave around −0.97 V vs $Fc^{+/0}$, a position that is within the broad range typical for the $Cu^{II/I}$ redox couple in copper complexes.[44] The corresponding anodic wave is extremely broad and shifted to −0.14 V. The three redox couples of the ligand occur at $E_{1/2}$ values of 0.10, 0.26, and 0.41 V. Similarly to the situation in the free ligand, these redox processes seem to be reversible. However, coordination leads to a large shift toward higher potentials, signaling a strong metal−ligand interaction. The potentials measured for the ligand-centered redox processes for $3(CuCl_2)_3$ and $3(CuI_2)_3$ are similar (see Figure S13b in the Supporting Information), but the wave assigned to metal reduction occurs at −0.55 V vs $Fc^{+/0}$ for $3(CuI_2)_3$ and is thus shifted to higher potentials compared with that of $3(CuCl_2)_3$. This result meets the expectation that copper reduction in the more electron-rich $3(CuI_2)_3$ complex is easier than that in the less electron-rich $3(CuCl_2)_3$ complex and lends support to the assignment of metal- and ligand-centered redox events.

Using the Evans method, the molar susceptibility of $3(CuCl_2)_3$ in CD_2Cl_2 solution was estimated from the nuclear magnetic resonance (NMR) chemical shifts to be 5.15×10^{-3} cm^3 mol^{-1}. The effective magnetic moment, μ_{eff}, was estimated to be 3.53 μ_B (see Table 3). Electron paramagnetic resonance (EPR) spectra of the complexes $3(CuX_2)_3$ (X = Cl, Br, or I), measured at room temperature in CH_2Cl_2 solution (ca. 1 mg/mL), are compared in Figure 8a. At room temperature, the copper fine structure is not visible. It can be seen that the signal broadens in the order X = Cl, Br, and I, and the g value slightly decreases. This trend might point to an increasing degree of spin delocalization. The calculated spin density in the complex $3(CuI_2)_3$ is illustrated in Figure 8b, and it can be seen that considerable spin density resides on the guanidino groups. According to a Mulliken population analysis for $3(CuCl_2)_3$ and $3(CuI_2)_3$, as much as 15.5% and 11.5%, respectively, of the difference in occupation numbers between α and β electrons is located on ligand **3**. Only 56.5% for $3(CuCl_2)_3$ and 42.5% for $3(CuI_2)_3$ of the surplus of α electrons is located at the copper atoms, following the trend in g values. This result fits with the coordination geometries at the copper atoms, which are between square-planar and tetrahedral, and also with the larger dihedral angles in $3(CuI_2)_3$ compared with $3(CuCl_2)_3$ (see the discussion of the crystal structures above). Consequently, the Cl and I atoms in $3(CuCl_2)_3$ and $3(CuI_2)_3$ carry 28% and 46%, respectively, of the surplus of α electrons. Hence, the iodine atoms clearly exhibit more radical character than the chlorine atoms, in line with the general instability of CuI_2 complexes with respect to CuI and I_2 (see discussion above). The Mulliken charges follow the same trend [0.38 and −0.40 e for the Cu and Cl atoms, respectively, in $3(CuCl_2)_3$ and 0.27 and −0.38 e for the Cu and I atoms, respectively, in $3(CuI_2)_3$]. Superconducting quantum interference device (SQUID) magnetometric measurements were carried out to study the temperature-dependent magnetism. Magnetization curves were measured at applied fields of 0.5, 1, 2, 3, 4, and 5 T and corrected for the underlying diamagnetism (see Figure 8c). The usual χT versus T plots, which were used to obtain the Curie−Weiss temperature (Θ_{CW}) and the temperature-independent paramagnetism (TIP), are provided in Figure S14 in the Supporting Information. The magnetization curves for all fields

Table 3. Summary of the Results of Magnetic Measurements[a]

	$[3(CuCl_2)_3]$	$[3(CuBr_2)_3]$	$[3(CuI_2)_3]$	$[3(CoCl_2)_3]$
$g_1=g_2=g_3$	2.093 (2.086[b])	2.086 (2.077[b])	2.032 (2.072[b])	2.550
$J_1 = J_2 = J_3$ (cm^{-1})	0.24	0.35	1.46	0.03
$D_1 = D_2 = D_3$ (cm^{-1})	–	–	–	46.96
$E/D_1 = E/D_2 = E/D_3$	–	–	–	−0.28
Θ_{CW} (K)	−0.53	−1.41	−3.80	−0.61
TIP (10^{-6} cm^3 mol^{-1})	6.5	3.9	1.8	12.3
μ_{eff} (1000 Oe)	3.64 (3.53[c])	3.60	4.17	7.36 (7.65[c])

[a]For more details, see the Supporting Information. [b]From electron paramagnetic resonance (EPR) spectroscopy. [c]μ_{eff} from Evans NMR analysis.

dx.doi.org/10.1021/ic501482u | Inorg. Chem. 2014, 53, 9876−9896

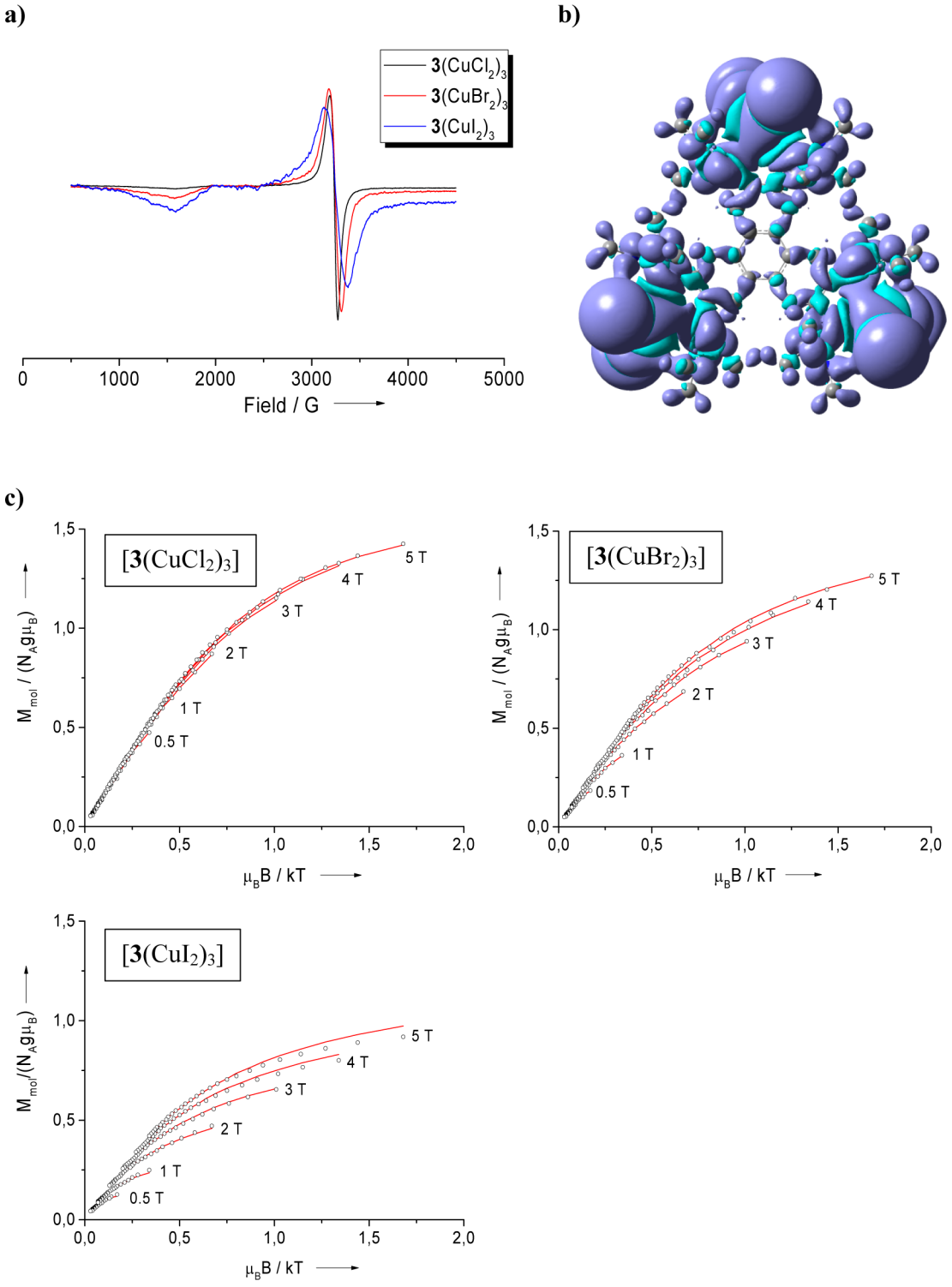

Figure 8. (a) EPR spectra of the three complexes $\mathbf{3}(CuX_2)_3$ (X = Cl, Br, and I). (b) Calculated spin density for the high-spin state ($S = {}^3/_2$) of $\mathbf{3}(CuI_2)_3$ (isovalue of 0.00004). (c) Magnetization curves of the three complexes as measured by SQUID together with a curve fit (see text for details).

are almost identical for $\mathbf{3}(CuCl_2)_3$, but they differ significantly for $\mathbf{3}(CuI_2)_3$. This trend indicates an increasing degree of magnetic superexchange of the three spin centers. The curves were fitted with the help of the julX program (see Experimental Details). The spin Hamiltonian is generally expressed as the sum of the Heisenberg–Dirac–Van Vleck Hamiltonian H_{ex}, the contribution from zero-field splitting H_{ZFS}, and the Zeeman-interaction term H_{Zee}

$$H = H_{ex} + H_{ZFS} + H_{Zee}$$

with

dx.doi.org/10.1021/ic501482u | Inorg. Chem. 2014, 53, 9876–9896

$$H_{ex} = -2\sum_{i<j}^{ns} J_{ij}\vec{S_i}\cdot\vec{S_j}$$

$$H_{ZFS} = \sum_{i=1}^{ns} D_i\left[S_{z,i}^{\ 2} - \frac{1}{3}S_i(S_i+1) + \frac{E_i}{D_i}(S_{x,i}^{\ 2} - S_{y,i}^{\ 2})\right]$$

and

$$H_{Zee} = \sum_{i=1}^{ns} g[\beta\vec{S_i}\cdot\vec{B}]$$

where J_{ij} is the magnetic coupling constant of local spin centers i and j; ns is the number of spins on each local spin center; and D_i and E_i/D_i are the local axial and rhombic zero-field splitting parameters, respectively.

For the copper complexes, the term H_{ZFE} is zero, as each local spin center is an $S = {}^1/_2$ system. In the fit, we assumed that all three metals have equal isotropic Landé factors g. In addition, the three isotropic coupling parameters J in the trinuclear complex were assumed to be similar. These assumptions are motivated by the structural data, which show that all of the metals are coordinated in similar ways. For all complexes, the coupling constant J turned out to be positive and to follow the order $\mathbf{3}(CuI_2)_3$ (J = 1.46 cm^{-1}) > $\mathbf{3}(CuBr_2)_3$ (J = 0.35 cm^{-1}) > $\mathbf{3}(CuCl_2)_3$ (J = 0.24 cm^{-1}). The g value follows the opposite trend, namely, $\mathbf{3}(CuI_2)_3$ (g = 2.032) < $\mathbf{3}(CuBr_2)_3$ (g = 2.086) < $\mathbf{3}(CuCl_2)_3$ (g = 2.093 cm^{-1}), in line with the results of the EPR measurements. In the past, we extensively studied the spin delocalization into the guanidino groups of paramagnetic bisguanidine and GFA complexes and also analyzed the effect of spin polarization on the aromatic backbone of bisguanidine ligands, leading to alternating low- and high-field shifts of the NMR signals.[45,46] Direct spin delocalization and spin polarization should both be of importance in the magnetic coupling of $\mathbf{3}(CuX_2)_3$ complexes.[47] The spin delocalization from the copper atoms into the guanidino groups depends on the Cu—N bond properties (covalent character and bond strength) and the angle between the N=C π-orbitals and the Cu magnetic orbital.[47,48] The Cu—N bond distances in $\mathbf{3}(CuCl_2)_3$ and $\mathbf{3}(CuI_2)_3$ are similar [on average, 1.972 Å in $\mathbf{3}(CuCl_2)_3$ and 1.974 Å in $\mathbf{3}(CuI_2)_3$], but of course the covalency differs. Presumably, the dihedral angle between the X—Cu—X and N—Cu—N planes is of higher importance for the magnetic coupling, because large dihedral angles [on average, 47° in $\mathbf{3}(CuCl_2)_3$ and 55° in $\mathbf{3}(CuI_2)_3$] must favor spin delocalization (see also the discussion in ref 47). For comparison, our B3LYP/def2-SV(P) calculations predict these angles to be 55° in $\mathbf{3}(CuCl_2)_3$ and 62° in $\mathbf{3}(CuI_2)_3$. The quantum chemical calculations argue for significant spin delocalization into the guanidino groups (see the plotted spin density in Figure 8b). From there, the magnetic coupling could be mediated by either direct spin delocalization or spin polarization. Spin polarization leads to an alternating sign of the spin on the ring carbon atoms. Indeed, some alternation of the spin on the central C_6 ring of the triphenylene unit could be observed (see Figure 8b).

We extended the analysis of trinuclear paramagnetic compounds of **3** by synthesizing and characterizing the complexes $\mathbf{3}(NiCl_2)_3$, $\mathbf{3}(NiBr_2)_3$, and $\mathbf{3}(CoCl_2)_3$, which exhibit six or nine unpaired electrons. Figure 9a,b displays the molecular structure of $\mathbf{3}(NiCl_2)_3$. All Ni atoms are symmetrically coordinated by two imino N atoms, and the average Ni—N distance measures 2.001 Å. Coordination leads to elongation of the N=C bond distances within the guanidino groups to an average value of 1.337 Å. The tetrahedral angles between the

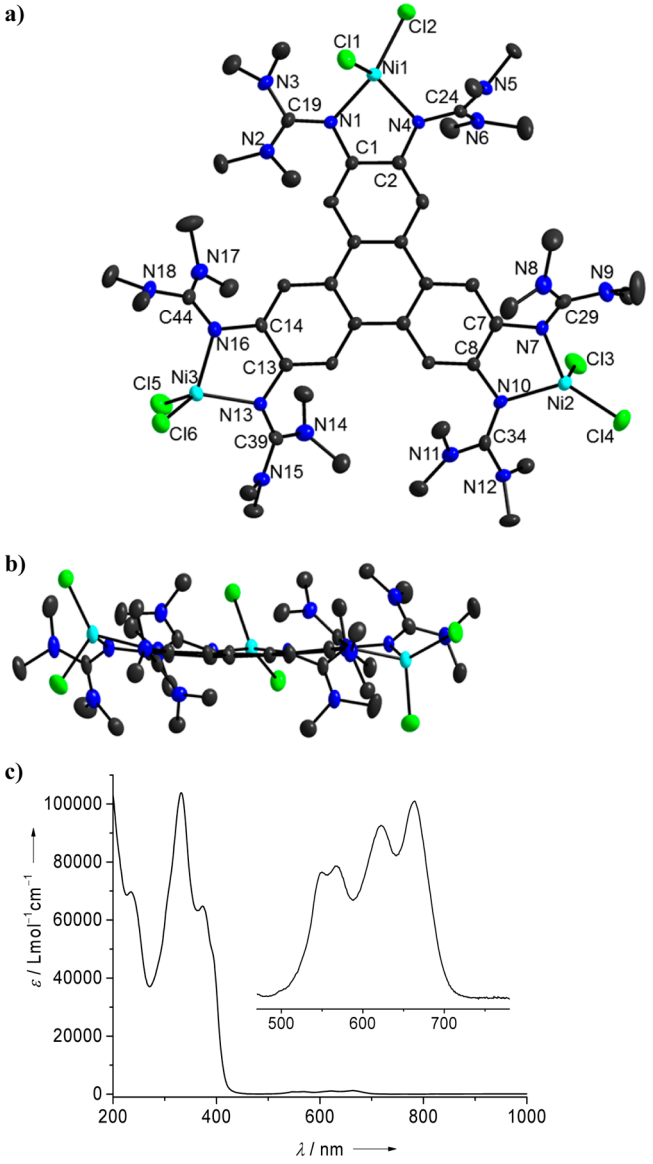

Figure 9. (a) Molecular structure of the trinuclear complex $\mathbf{3}(NiCl_2)_3$. Vibrational ellipsoids drawn at the 50% probability level. Hydrogen atoms omitted for the sake of clarity. Selected bond distances (in Å) and angles (in deg): Ni1—Cl1 2.2483(15), Ni1—Cl2 2.2401(17), Ni2—Cl3 2.2556(16), Ni2—Cl4 2.2380(15), Ni3—Cl5 2.2551(17), Ni3—Cl6 2.2341(16), Ni1—N1 2.004(4), Ni1—N4 1.986(4), Ni2—N7 1.993(4), Ni2—N10 2.023(4), Ni3—N13 1.996(4), Ni3—N16 2.005(4), N1—C1 1.410(6), N1—C19 1.339(6), N2—C19 1.343(7), N3—C19 1.346(6), N4—C2 1.405(6), N4—C24 1.353(6), N5—C24 1.341(6), N6—C24 1.345(7), N7—C7 1.404(6), N7—C29 1.325(6), N8—C29 1.365(7), N9—C29 1.340(6), N10—C8 1.401(5), N10—C34 1.330(6), N11—C34 1.369(6), N12—C34 1.344(6), N13—C13 1.419(6), N13—C39 1.343(6), N14—C39 1.349(7), N15—C39 1.345(6), N16—C14 1.413(6), N16—C44 1.333(6), N17—C44 1.329(7), N18—C44 1.359(7), Cl1—Ni1—Cl2 106.54(6), Cl3—Ni2—Cl4 113.59(6), Cl5—Ni3—Cl6 113.56(7), N1—Ni1—N4 83.12(15), N7—Ni2—N10 82.63(15), N13—Ni3—N16 83.15(16). (b) View from a different perspective showing the coordination mode. (c) UV/vis spectrum of $\mathbf{3}(NiCl_2)_3$ in CH_3CN solution.

dx.doi.org/10.1021/ic501482u | Inorg. Chem. 2014, 53, 9876−9896

Cl—Ni—Cl and N—Ni—N planes through the two Ni atoms are different. The tetrahedral angle at Ni1 measures 65.0°, whereas the tetrahedral angles at Ni2 and Ni3 are close to 90° (89.7° and 89.4°, respectively). The structure of $\mathbf{3}(CoCl_2)_3$ was also measured (see Figure S15 in the Supporting Information). Again, two dihedral planes (Cl—Co—Cl, N—Co—N) are close to the expected value of 90° (88.9° and 89.5° at Co1 and Co3, respectively), whereas the third is significantly smaller (67.3°). The UV/vis spectrum provided evidence for d−d transitions at 684, 580, and 512 nm for $\mathbf{3}(NiCl_2)_3$ (see Figure 9c). As expected, the bands shift to slightly larger values of 708, ca. 607, and ca. 539 nm for $\mathbf{3}(NiBr_2)_3$ (see Experimental Details). For $\mathbf{3}(CoCl_2)_3$, d−d transitions were detected at 664, 622, 568, and 550 nm (see Figure S16 in the Supporting Information). A first analysis by NMR spectrocsopy using the Evans method gave molar susceptibilities of 7.7958×10^{-3} and 2.4163×10^{-2} cm^3 mol^{-1} for $\mathbf{3}(NiCl_2)_3$ and $\mathbf{3}(CoCl_2)_3$, respectively. The effective magnetic moments, μ_{eff}, were estimated to be 4.35 and 7.65 μ_B, respectively, for the two complexes. Using SQUID, a μ_{eff} value of 7.36 μ_B was obtained for $\mathbf{3}(CoCl_2)_3$, in pleasing agreement with the value estimated in solution by the Evans method (see Table 3). Magnetization curves were recorded for $\mathbf{3}(CoCl_2)_3$ and fitted using the following parameters: $g = 2.55$, $J = 0.029$ cm^{-1}, $D = 47.0$ cm^{-1} (all axial zero-field splitting parameters D were assumed to be equal), $E/D = -0.28$, together with a temperature-independent paramagnetism (TIP) of 12.3×10^{-6} cm^3 mol^{-1} (see Figure S16b in the Supporting Information). Hence, the magnetic coupling between the three spin centers is very weak, whereas the zero-field splitting parameter D is relatively large (see a discussion for other mono- and dinuclear guanidine complexes in ref 49).

Coordination as a Means to Form Arrays of 3. The new organic electron donors could be linked by coordinative bonds to highly ordered arrays. We started our studies in this area with the reaction beween **3** and AgCN and obtained a molecular coordination compound, namely, the trinuclear complex $\mathbf{3}(AgCN)_3$. Its crystal structure is shown in Figure 10. All three silver atoms are 3-fold-coordinated. By contrast, reaction with silver halides AgX (X = Cl, Br, or I) led to coordination polymers $[\mathbf{3}(AgX)_3]_n$. All three compounds crystallized, and the structures of $[\mathbf{3}(AgCl)_3]_n$ and $[\mathbf{3}(AgI)_3]_n$ are illustrated in Scheme 7 and Figures 11 and 12 {see Figure S17 In the Supporting Information for the structure of $[\mathbf{3}(AgBr)_3]_n$}. Some degree of disorder of the silver and halogen atoms occurs, especially in the case of $[\mathbf{3}(AgI)_3]_n$ (see Figure 12). An interesting detail of all structures is the massive displacement of the tetrahedrally coordinated Ag atoms from the aromatic plane of the ligand. In $[\mathbf{3}(AgCl)_3]_n$, for example, the two tetrahedrally coordinated Ag atoms are displaced by as much as 1.489 Å (Ag1) and 1.375 Å (Ag2) from the best plane of the triphenylene core (see Figure 11). By contrast, the trigonally coordinated third Ag atom is displaced by not more than 0.009 Å from this plane. As in $\mathbf{3}(AgCN)_3$, the triphenylene core exhibits a curled structure. For X = Cl or Br, only two of the three Ag atoms of each complex unit establishes connections to the next complex units through halogen bridges. Hence, the structure features both tetrahedrally and trigonally coordinated Ag atoms. In the case of $[\mathbf{3}(AgI)_3]_n$, all three Ag atoms are 4-fold-coordinated and connected through halogen bridges to the next complex units (see Figure 12a). Such a connectivity pattern leads to layers with a honeycomb structure, consisting of hexagons built of six complex units. The arrangement of the layers is shown in Figure 12b and results in a porous structure that has some similarities to (but also differences from) the experimentally verified or predicted structures obtained with other triphenylene derivatives.[8] Using the program CrystalExplorer, the pore volume per unit cell was estimated to be 1644.5 $Å^3$, and the pore volume per gram was estimated to be 0.15365 cm^3 g^{-1} (see Figure S18 in the Supporting Information for the visualization of the voids).[50] This is a quite high value

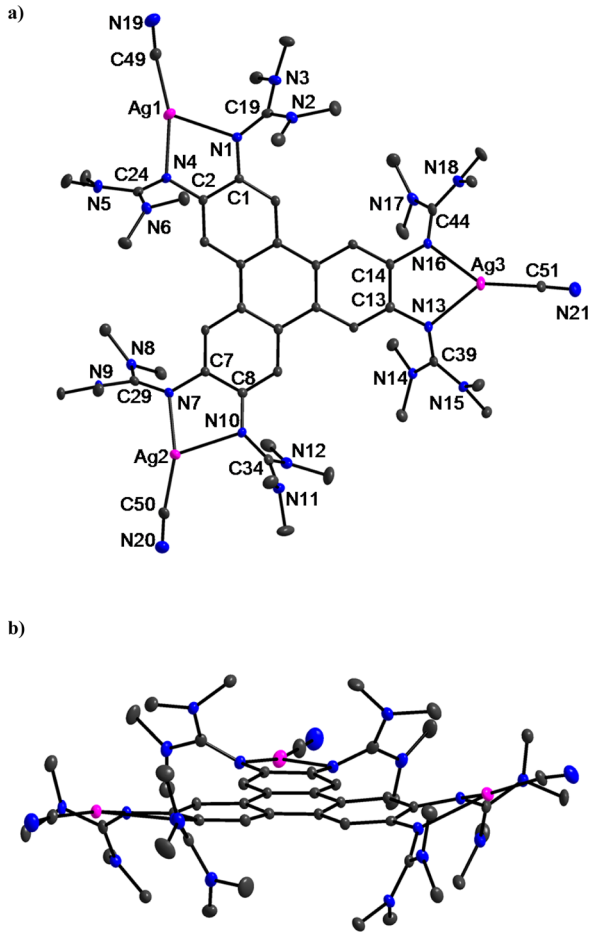

Figure 10. (a) Molecular structure of the trinuclear complex $\mathbf{3}(AgCN)_3$. Vibrational ellipsoids drawn at the 50% probability level. Hydrogen atoms omitted for the sake of clarity. Selected bond distances (in Å) and angles (in deg): Ag1—N1 2.353(5), Ag1—N4 2.202(5), Ag1—C49 2.062(8), Ag2—N7 2.184(5), Ag2—N10 2.382(5), Ag2—C50 2.037(7), Ag3—N13 2.311(5), Ag3—N16 2.261(5), Ag3—C51 2.063(7), N1—C1 1.400(8), N1—C19 1.317(9), N2—C19 1.359(9), N3—C19 1.374(8), N4—C2 1.418(7), N4—C24 1.339(8), N5—C24 1.373(8), N6—C24 1.351(9), N7—C7 1.411(8), N7—C29 1.328(8), N8—C29 1.367(8), N9—C29 1.366(8), N10—C8 1.398(8), N10—C34 1.306(8), N11—C34 1.350(9), N12—C34 1.367(9), N13—C13 1.419(8), N13—C39 1.314(8), N14—C39 1.367(8), N15—C39 1.356(8), N16—C14 1.419(8), N16—C44 1.311(8), N17—C44 1.374(9), N18—C44 1.358(9), N19—C49 1.132(10), N20—C50 1.137(9), N21—C51 1.121(9), C1—C2 1.414(8), C7—C8 1.414(8), C13—C14 1.419(9), N1—Ag1—N4 74.87(19), N1—Ag1—C49 121.4(3), N4—Ag1—C49 163.0(3), Ag1—C49—N19 170.8(8), N7—Ag2—N10 73.94(18), N7—Ag2—C50 163.5(2), N10—Ag2—C50 120.9(2), Ag2—C50—N20 171.5(7), N13—Ag3—N16 73.86(18), N13—Ag3—C51 138.8(2), N16—Ag3—C51 147.1(2), Ag3—C51—N21 172.0(8). (b) View from a different perspective showing the curled structure of the triphenyl system.

dx.doi.org/10.1021/ic501482u | Inorg. Chem. 2014, 53, 9876−9896

Scheme 7. Lewis Structures of the Complex Units and Their Connectivity in the Chain Polymer $[3(AgCl)_3]_n$[a] and in One of the Sheets of the Porous Polymer $[3(AgI)_3]_n$

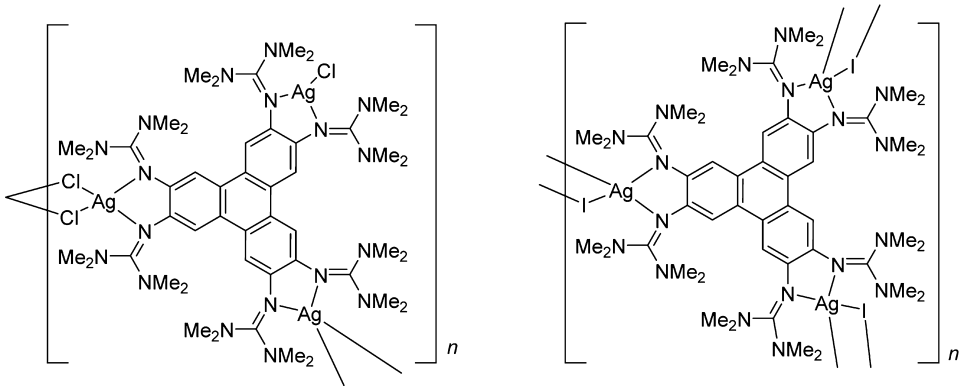

[a]Similar structure for $[3(AgBr)_3]_n$.

(see the discussion in ref 50b). Only a small amount of crystalline material was obtained (according to powder XRD measurements, the pure material obtained directly upon removal of the solvent was amorphous), so that we have thus far not been able to estimate the pore volume from gas absorption experiments. In ongoing experiments, we are collecting more crystalline material to study the possibility of intercalation into the layer structure of $[3(AgI)_3]_n$. Because of the redox activity of the organic linkers in this coordination polymer, oxidizing guest molecules such as I_2 are at the center of interest in this effort.

CONCLUSIONS

The new redox-active ligands 2,3,6,7,10,11-hexakis-(tetramethylguanidino)triphenylene (**3**) and 2,3,6,7,10,11-hexakis(dimethylethyleneguanidino)triphenylene (**4**) were prepared in four steps starting from triphenylene. Their redox activity was analyzed and compared to that of 1,2,4,5-tetrakis(tetramethylguanidinyl)benzene (**1**). CV measurements showed that they could be oxidized reversibly in three two-electron steps, and the possible structures of the oxidized species were discussed on the basis of quantum chemical calculations. With $E_{1/2} = -0.39$ V vs $Fc^{+/0}$ for the first two-electron redox event in CH_2Cl_2 solution, its electron-donor capacity is lower than that of **1** (−0.76 V vs $Fc^{+/0}$). On the other hand, quantum chemical calculations predict the gas-phase reduction of $\mathbf{1}^{2+}$ with **3** to give **1** and $\mathbf{3}^{2+}$ to be associated with a Gibbs free energy change of almost zero, which implies that the intrinsic or gas-phase electron-donor capacities are similar for **3** and **1**. This result highlights the massive difference between intrinsic and experienced electron-donor capacities, which mainly arises from the solvent stabilization of the charged species. The new redox-active triphenylene derivative **3** can be evaporated without decomposition.

This work concentrated on the coordination chemistry of the new guanidino-functionalized aromatic (GFA) compound **3**. Trinuclear Cu^I and Cu^{II} complexes were prepared, and their structures and electronic properties were compared. The special complex $3(CuI_2)_3$ can be obtained by oxidation of $3(CuI)_3$ with I_2. Whereas the triphenylene core in the Cu^I complexes is curled, it is planar in the Cu^{II} complexes. In the Cu^I complexes, the metals are trigonal-planar-coordinated, and in the Cu^{II} complexes, the coordination is intermediate between square-planar and tetrahedral. With the help of TD-DFT calculations, some characteristic bands in the electronic absorption spectra were assigned to metal-to-ligand charge-transfer (MLCT) transitions (for the Cu^I complexes) or LMCT transitions (for the Cu^{II} complexes). The magnetic coupling in the Cu^{II} complexes was studied by SQUID magnetometric measurements, and the data indicated weak ferromagnetic coupling between the three spin centers that increases within the series $3(CuCl_2)_3 < 3(CuBr_2)_3 < 3(CuI_2)_3$. The unusual coordination of the copper atoms [the dihedral angles between the X—Cu—X (X = halogen) and N—Cu—N planes measure, on average, 47° for $3(CuCl_2)_2$ and 55° for $3(CuI_2)_3$] enables considerable spin delocalization into the guanidino groups. We extended our analysis to a trinuclear Co complex of **3** that exhibits a high *D* value (zero-field splitting) and a very weak (ferromagnetic) coupling between the spin centers, as well as to Ni complexes.

Finally, we showed that redox-active **3** can be integrated into coordination polymers by reaction with silver halides. With AgCl or AgBr, chain polymers $[3(AgCl)_3]_n$ or $[3(AgBr)_3]_n$, respectively, are formed, in which two of the three silver atoms of each complex unit are linked by halogen bridges to the next complex unit, whereas the third silver atom is trigonal-planar-coordinated without establishing a link to the next complex unit. In the case of AgI, the porous material $[3(AgI)_3]_n$ results (with an estimated pore volume per unit cell and per gram of 1644.5 Å^3 and 0.15365 cm^3 g^{-1}, respectively), which consists of sheets in which all three silver atoms of each complex unit are linked by halogen bridges to the adjacent complex units. In this way, a honeycomb structure results, composed of hexagons formed from six complex units. In all of these structures, the silver atoms are heavily displaced from the "best plane" of the triphenylene cores. In ongoing work, we are testing the possibility of intercalating redox-active guest molecules into the layer structure of $[3(AgI)_3]_n$.

EXPERIMENTAL DETAILS

General Procedures. All reactions were carried out under inert gas atmosphere using standard Schlenk techniques. NMR spectra were measured on a DRX-200 or a Bruker Avance III 600 spectrometer. UV/vis spectra were recorded using a Cary 5000 spectrophotometer. For IR spectroscopy, CsI disks of the compounds were measured with an FTIR Biorad Merlin Excalibur FT 3000 spectrometer. Elemental analyses were carried out at the Microanalytical Laboratory of the University of Heidelberg. An EG&G Princeton 273 apparatus was used for the CV measurements. The curves were recorded at different scan rates in the range of 50−200 mV s^{-1} with an Ag/AgCl electrode as the

dx.doi.org/10.1021/ic501482u | Inorg. Chem. 2014, 53, 9876−9896

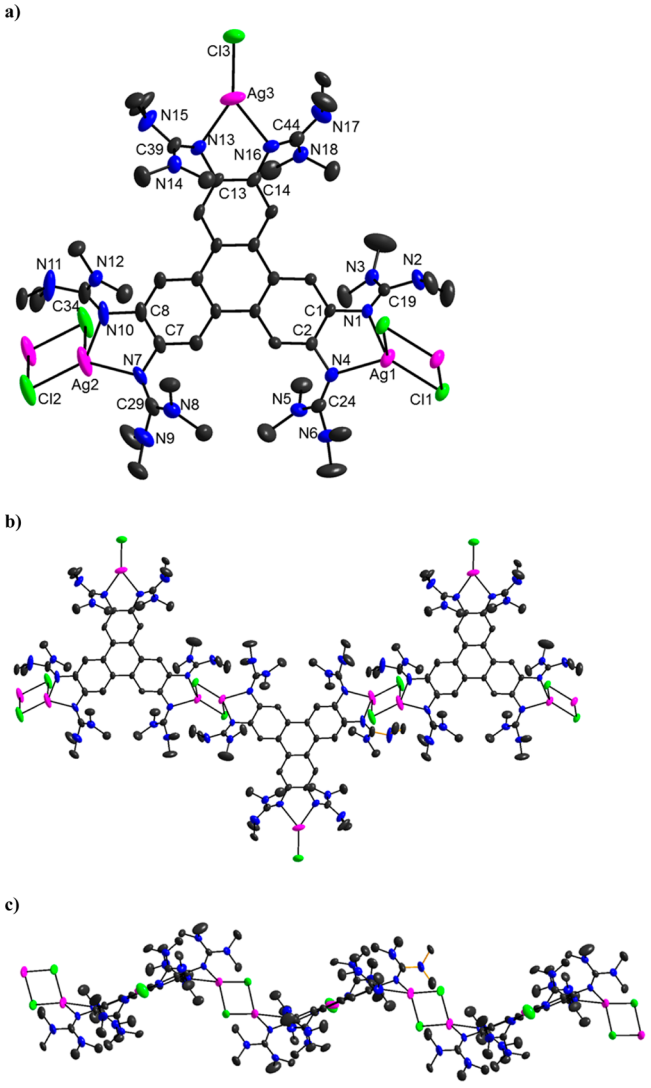

Figure 11. Structure of the coordination polymer $[\mathbf{3}(AgCl)_3]_n$. Vibrational ellipsoids drawn at the 50% probability level. Hydrogen atoms omitted for the sake of clarity. (a) One of the triphenylene units and the silver chloride coordination. Selected bond distances (in Å) and angles (in deg): Ag1—Cl1 2.4549(15), Ag1—Cl1′ 2.7913(18), Ag1—N1 2.332(5), Ag1—N4 2.380(5), Ag2—Cl2 2.448(2), Ag2—Cl2′ 2.832(2), Ag2—N7 2.327(5), Ag2—N10 2.372(7), Ag3—Cl3 2.336(2), Ag3—N13 2.256(5), Ag3—N16 2.315(5), N1—C1 1.398(6), N1—C19 1.316(7), N2—C19 1.373(7), N3—C19 1.356(7), N4—C2 1.391(7), N4—C24 1.334(8), N5—C24 1.357(8), N6—C24 1.362(8), N7—C7 1.413(8), N7—C29 1.329(9), N8—C29 1.362(9), N9—C29 1.354(9), N10—C8 1.410(7), N10—C34 1.321(10), N11—C34 1.390(8), N12—C34 1.366(10), Cl1—Ag1—Cl1′ 96.15(5), Cl2—Ag—Cl2′ 93.07(7), N1—Ag1—N4 71.69(16), N7—Ag2—N10 71.7(2), N13—Ag3—N16 74.22(18). (b) Visualization of one of the chains. Two of the Ag atoms attached to each triphenylene are tetrahedrally coordinated, and the third one is trigonally coordinated. (c) View parallel to the triphenylene plane highlighting the displacement of the silver atoms from the aromatic plane.

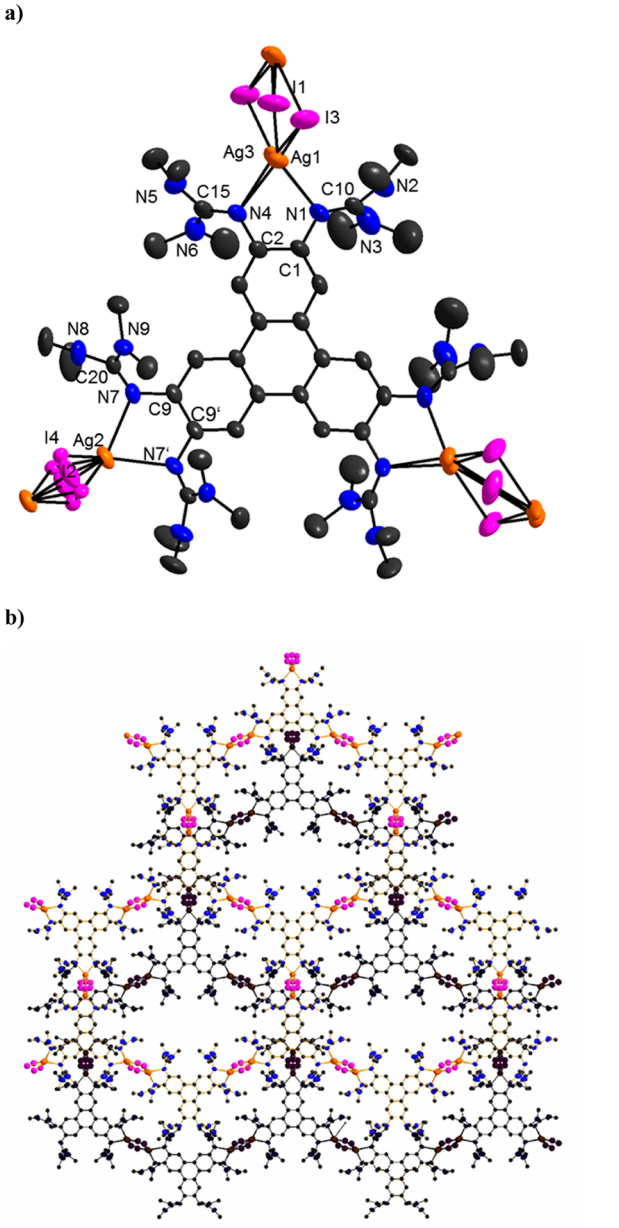

Figure 12. (a) Structure of the coordination polymer $[\mathbf{3}(AgI)_3]_n$. The iodine atoms are heavily disordered. Vibrational ellipsoids drawn at the 50% probability level. Hydrogen atoms omitted for the sake of clarity. Selected bond distances (in Å) and angles (in deg): Ag1—I1 2.7306(17), Ag1—I1′ 2.9239(17), Ag2—I2 2.8179(19), Ag2—I4 2.745(2), Ag3—I3′ 2.756(3), Ag3—I3 2.866(5), Ag1—N1 2.333(8), Ag1—N4 2.359(5), Ag2—N7 2.383(5), Ag3—N1 2.474(8), Ag3—N4 2.307(6), N1—C1 1.395(9), N1—C10 1.263(10), N2—C10 1.327(10), N3—C10 1.414(13), N4—C2 1.425(9), N4—C15 1.316(9), N5—C15 1.366(11), N6—C15 1.383(12), N7—C9 1.407(7), N7—C20 1.310(8), N8—C20 1.385(8), N9—C20 1.340(9), I1—Ag1—I1′ 99.46(5), I3—Ag3—I3′ 105.04(12), I4—Ag2—I4′ 106.07(5), N1—Ag1—N4 73.0(2), N1—Ag3—N4 71.3(2), N7—Ag2—N7′ 73.3(2). (b) Illustration of the layer structure of the material. Two layers are shown (top layer in color and bottom layer in gray).

reference electrode and Bu_4NPF_6 (Fluka, electrochemical grade) as the electrolyte. For the SQUID direct-current (dc) measurements, a Quantum Design MPMS-XL 5 instrument was used. The SQUID magnetometric data were analyzed with the help of the julX program.[51] High-resolution electrospray ionization (HR-ESI) spectra were recorded on a Finnigan LCQ quadrupole ion trap. High-resolution fast atom bombardment (HR-FAB) and liquid-injection field desorption/ionization (LIFDI) spectra were recorded on a JEOL JMS-700 magnetic sector.

Materials. All solvents were dried with an MBraun Solvent Purification System prior to their use. 2,3,6,7,10,11-Hexaaminotriphenylene was synthesized according to the literature method.[33]

dx.doi.org/10.1021/ic501482u | Inorg. Chem. 2014, 53, 9876−9896

Triphenylene was purchased from Aldrich (98%) and used as delivered. The CuI salts CuCl and CuBr; the AgI salts AgCl, AgBr, and AgCN; and the salts Ni(dme)Cl_2 (dme = dimethoxyethane), Ni(dme)Br_2, and $CoCl_2$ were purchased from ABCR. AgI, CuCN, and CuI were purchased from Strem and Aldrich, respectively. The Cu^{II} salts $CuCl_2$ and $CuBr_2$ were obtained from Riedel-de Haën.

Synthesis of 2,3,6,7,10,11-Hexaaminotriphenylene·6HCl. The synthesis started with the preparation of 2,3,6,7,10,11-hexabromotriphenylene according to a literature protocol,[32] which was further converted to the hydrochloride of 2,3,6,7,10,11-hexaaminotriphenylene.[33]

Synthesis of 2-Chloro-1,1′,3,3′-tetramethylformamidinium Chloride (Activated Urea). *N*,*N*,*N*′,*N*′-Tetramethylurea (0.670 mL, 0.648 g, 5.581 mmol) was dissolved in 20 mL of $CHCl_3$. Subsequently, oxalyl chloride (2.436 mL, 3.545 g, 27.926 mmol, 30 equiv) was added slowly dropwise, and the reaction mixture was stirred under reflux for a period of 16 h. The solvent was removed under a vacuum, and the remaining solid was washed three times with 6 mL portions of Et_2O. Finally, the solid was dried and dissolved in 15 mL of CH_3CN. This solution was used without further analysis for the preparation of ligand **3**.

Synthesis of 2,3,6,7,10,11-Hexakis(tetramethylguanidino)-triphenylene, 3. The solution of 2-chloro-1,1′,3,3′-tetramethylformamidinium chloride was slowly added to a suspension of 2,3,6,7,10,11-hexaaminotriphenylene·6HCl (0.500 g, 0.931 mmol) in 15 mL of CH_3CN. Triethylamine (2.225 mL, 1.696 g, 16.756 mmol, 18 equiv) was slowly added to the reaction mixture at a temperature of 0 °C. Then, the suspension was stirred for a period of 4 h at 0 °C, during which time it turned red-brown. The red-brown solid obtained after removal of the solvent under a vacuum was redissolved in a 10% aqueous HCl solution (15 mL). Subsequently, a 25% aqueous NaOH solution (15 mL) was added. The solution was extracted with toluene until the organic phase remained colorless. The combined organic phases were dried over K_2CO_3, and the solvent was removed under a vacuum. Recrystallization of the crude product from CH_3CN yielded 0.784 g (0.864 mmol, 93%) of **3** in the form of a beige-colored solid. The product was further purified by sublimation and was then isolated as a pale-yellow-colored solid. Elemental analysis for $C_{48}H_{78}N_{18}$ (907.35): calcd C 63.54, H 8.67, N 27.79; found C 62.95, H 8.60, N 27.45. HR-FAB$^+$: m/z = 907.6757 [**3** + H]$^+$, 100%, calcd 907.6753; 906.6691 [**3**]$^+$, 44.4%, calcd 906.6657; 862.6138 [**3** − NMe_2]$^+$, 26.8%, calcd 862.6157. ^{1}H NMR (600.13 MHz, CD_3CN): δ = 7.31 (s, 6H, H_{arom}), 2.69 (s, 72H, CH_3) ppm. $^{13}C\{^1H\}$ NMR (150.90 MHz, CD_3CN), HSQC, HMBC: δ = 159.19 (N═C), 144.79 (C_{arom}), 124.48 (C_{arom}), 114.20 (CH_{arom}), 39.95 (CH_3) ppm. ^{1}H NMR (600.13 MHz, C_6D_6): δ = 8.08 (s, 6H, H_{arom}), 2.57 (s, 72H, CH_3) ppm. $^{13}C\{^1H\}$ NMR (150.90 MHz, C_6D_6), HSQC, HMBC: δ = 158.08 (N═C), 144.30 (C_{arom}), 125.44 (C_{arom}), 114.77 (CH_{arom}), 39.75 (CH_3) ppm. ^{1}H NMR (600.13 MHz, CD_2Cl_2): δ = 7.37 (s, 6H, H_{arom}), 2.71 (s, 72H, CH_3) ppm. $^{13}C\{^1H\}$ NMR (150.90 MHz, CD_2Cl_2), HSQC, HMBC: δ = 158.17 (N═C), 143.41 (C_{arom}), 123.47 (C_{arom}), 113.34 (CH_{arom}), 39.15 (CH_3) ppm. IR (CsI): ν = 2997 (w), 2926 (m), 2886 (m), 2804 (w), 1594 (s), 1483 (s), 1457 (m), 1424 (m), 1408 (m), 1373 (s), 1294 (w), 1232 (m), 1220(m), 1137 (s), 1062 (w), 1027 (s), 986 (m), 922 (w), 874 (m), 833 (w), 788 (w), 763 (w), 747 (w), 736 (w), 701 (w), 669 (w), 630 (w), 599 (w) cm^{-1}. UV/vis (CH_3CN, c = 2.5793 × 10^{-5} mol/L, d = 0.5 cm): λ (ε, M^{-1} cm^{-1}) = ca. 215 (66076), 322 (94581), ca. 356 (45808) nm.

Synthesis of 3·6HCl. **3** (77.3 mg, 0.0852 mmol) was dissolved in 7 mL of Et_2O. Then, 0.51 mL of HCl·Et_2O (1 N solution, 0.5112 mmol, 6 equiv) was added. A colorless solid precipitated. After 1 h, the solvent was removed by filtration, and the solid washed three times with 3 mL portions of Et_2O. Finally, the product was dried to obtain 82.7 mg (0.0734 mmol, 86%) of **3**·6HCl, which was recrystallized from a CH_3CN solution. **3**·6HCl·3H_2O, $C_{48}H_{90}N_{18}Cl_6O_3$ (1180.07): calcd C 48.85, H 7.69, N 21.36; found C 49.20, H 7.89, N 21.49. HR-ESI$^+$: m/z = 907.67279 ([**3** + H]$^+$, 78.6%, calcd 907.67296), 454.34018 ([**3** + 2H]$^{2+}$, 100.0%, calcd 454.34067). ^{1}H NMR (600.13 MHz, CD_3CN): δ = 11.31 (s, 6H, N—H), 8.38 (s, 6H, H_{arom}), 3.10 (s, 72H, CH_3) ppm. $^{13}C\{^1H\}$ NMR (150.90 MHz, CD_3CN), HSQC, HMBC: δ = 159.67 (N═C), 131.93 (C_{arom}), 128.49 (C_{arom}), 119.56 (CH_{arom}), 41.79 (CH_3) ppm. IR (CsI): ν = 3454 (m), 3209 (w), 3019 (w), 2963 (m), 2814 (w), 1637 (s), 1551 (s), 1470 (m), 1423 (s), 1405 (s), 1307 (s), 1261 (w), 1231 (m), 1171 (s), 1150 (m), 1106 (w), 1069 (m), 1047 (m), 1040 (w), 1012 (m), 923 (w), 900 (m), 796 (m) cm^{-1}. UV/vis (CH_3CN, c = 2.0229 × 10^{-5} mol/L, d = 0.5 cm): λ (ε, M^{-1} cm^{-1}) = ca. 332 (49599, shoulder), 303 (125182), 243 (49044) nm. Crystal data for [**3**H_6]Cl_6·5H_2O, $C_{48}H_{94}Cl_6N_{18}O_5$: M_r = 1216.11, 0.40 × 0.20 × 0.20 mm^3, monoclinic, space group $P2_1/n$, a = 16.938(3) Å, b = 12.940(3) Å, c = 30.764(6) Å, β = 90.87(3)°, V = 6742(2) Å^3, Z = 4, d_{calc} = 1.198 Mg·m^{-3}, Mo Kα radiation (graphite-monochromated, λ = 0.71073 Å), T = 100 K, θ_{range} 1.98−27.60°. Reflns measd 117363, indep 15489, R_{int} = 0.0671. Final R indices [$I > 2\sigma(I)$]: R1 = 0.0504, wR2 = 0.1234.

Synthesis of 2,3,6,7,10,11-Hexakis-(dimethylethylenguanidino)triphenylene, 4. 1,3-Dimethylimidazolidine-2-on (0.4218 mL, 0.4463 g, 3.9096 mmol) was dissolved in 20 mL of $CHCl_3$. Then, oxalyl chloride (1.7053 mL, 2.4812 g, 19.5480 mmol) was added dropwise. Subsequently, the mixture was heated to reflux for a period of 16 h. The solvent was removed under a vacuum, and the remaining solid was washed three times with 10 mL portions of Et_2O and then dissolved in 12 mL of CH_3CN. This solution was added to a suspension of 2,3,6,7,10,11-hexaaminotriphenylene hexahydrochloride (0.300 g, 0.5585 mmol) in 12 mL of CH_3CN, and NEt_3 (1.3350 mL, 1.0173 g, 10.0532 mmol) was slowly added at a temperature of 0 °C. The suspension was stirred for a period of 4.5 h, during which time the reaction mixture was allowed to warm from 0 °C to room temperature. The solution turned beige, and a bright solid formed. Subsequently, the solvent was removed under a vacuum to obtain a pale-brown-colored solid, which was dissolved in 18 mL of an aquous HCl solution (10%). After addition of 18 mL of NaOH (25%), the solution was extracted with CH_3CN until the organic phase remained colorless. The solvent was then removed in vacuo. Upon recrystallization of the raw product from CH_3CN, compound **4** was obtained as a beige-brown-colored solid. Yield: 0.282 g (0.3151 mmol, 56%). C $_{48}H_{66}N_{18}$ (895.16): calcd C 64.40, H 7.43, N 28.16; found C 63.18, H 7.27, N 27.27. HR-ESI$^+$ (MeOH): m/z = 895.57936 [**4** + H]$^+$, 12%, calcd 895.57961; 448.29314 [**4** + 2H]$^{2+}$, 100.0%, calcd 448.29372; 299.19790 [**4** + 3H]$^{3+}$, 9.2%, calcd 299.19842. ^{1}H NMR (600.13 MHz, CD_2Cl_2): δ = 7.66 (s, 6H, H_{arom}), 3.25 (s, 24H, CH_2), 2.67 (s, 36H, CH_3) ppm. $^{13}C\{^1H\}$ NMR (150.90 MHz, CD_2Cl_2), HSQC, HMBC: δ = 154.59 (N═C), 142.52 (C_{arom}), 124.22 (C_{arom}), 115.16 (CH_{arom}), 49.13 (CH_2), 35.23 (CH_3) ppm. IR (CsI): ν = 3048 (w), 2933 (w), 2844 (w), 2794 (w), 1650 (m), 1588 (m), 1482 (m), 1438 (m), 1415 (m), 1391 (s), 1281 (s), 1243 (s), 1233(s), 1198 (w), 1163 (m), 1137 (m), 1092 (w), 1075 (m), 1039 (s), 999 (m), 990 (w), 969 (s), 960 (s), 880 (s), 853 (w), 845 (w), 823 (w), 769 (m), 725 (m), 713 m), 680 (w), 669 (w), 646 (w), 610 (m), 595 (w), 586 (w) cm^{-1}. UV/vis (CH_2Cl_2, c = 2.6364 × 10^{-5} mol/L, d = 0.5 cm): λ (ε, M^{-1} cm^{-1}) = 317 (96675), ca. 354 (43032, shoulder) nm.

Synthesis of 4·3HCl. **4** (296.1 mg, 0.3308 mmol) was dissolved in 8 mL of CH_3CN, and 0.99 mL of HCl·Et_2O (2 N solution, 1.9847 mmol, 6 equiv) was added. Initially, the formation of a bright solid was observed, but it later disappeared. After the mixture had been stirred for a period of 1 h at room temperature, the solvent was removed, and the product was crystallized by slow diffusion of Et_2O into a CH_3CN solution of **4**·3HCl. A total of 170.3 mg (0.1609 mmol, 49%) of clean product (**4**·3HCl·3H_2O) was obtained. **4**·3HCl·3H_2O, $C_{48}H_{75}N_{18}Cl_3O_3$ (1058.59): calcd C 54.46, H 7.14, N 23.82; found C 53.43, H 7.12, N 23.99. HR-ESI$^+$ (CH_3CN): m/z = 895.58043 ([**4** + H]$^+$, 100.0%, calcd 895.57906), 448.29340 ([**4** + 2H]$^{2+}$, 51.1%, calcd 448.29317), 299.19808 ([**4** + 3H]$^{3+}$, 11.5%, calcd 299.19787). ^{1}H NMR (600.13 MHz, CD_3CN): δ = 10.92 (s, 3H, N—H), 8.16 (s, 6H, H_{arom}), 3.41 (s, 24H, CH_2), 2.71 (s, 36H, CH_3) ppm. $^{13}C\{^1H\}$ NMR (150.90 MHz, CD_3CN), HSQC, HMBC: δ = 157.35 (N═C), 118.43 (CH_{arom}), 49.30 (CH_2), 35.04 (CH_3) ppm. IR (CsI): ν = 3453 (m), 3236 (w), 3135 (w), 2937 (m), 2876 (m), 1632 (s), 1585 (s), 1491 (s), 1448 (s), 1419 (s), 1398 (s), 1376 (m), 1301 (s), 1289 (s), 1239 (m), 1142 (w), 1075 (w), 1040 (s), 1009 (m), 967 (s), 886 (w), 844 (w), 795 (w), 772 (w), 748 (w), 698 (m) cm^{-1}. UV/vis (CH_3CN, c =

dx.doi.org/10.1021/ic501482u | Inorg. Chem. 2014, 53, 9876−9896

1.2469 × 10^{-5} mol/L, d = 1.0 cm): λ (ε, M^{-1} cm^{-1}) = ca. 352 (42425, shoulder), 315 (79669) nm. Crystal data for $[\mathbf{4}H_3]Cl_3{\cdot}H_2O{\cdot}CH_3CN$, $C_{50}H_{74}Cl_3N_{19}O$: M_r = 1063.63, 0.40 × 0.35 × 0.20 mm^3, monoclinic, space group $P2_1/c$, a = 8.599(2) Å, b = 26.487(5) Å, c = 24.255(5) Å, β = 96.62(3)°, V = 5487.5(19) $Å^3$, Z = 4, d_{calc} = 1.287 $Mg{\cdot}m^{-3}$, Mo Kα radiation (graphite-monochromated, λ = 0.71073 Å), T = 100 K, θ_{range} 2.29−27.46°. Reflns measd 24582, indep 12516, R_{int} = 0.0276. Final R indices [$I > 2\sigma(I)$]: R1 = 0.0465, wR2 = 0.1235.

Synthesis of [3(CuCN)$_3$]. CuCN (29.9 mg, 0.3340 mmol, 3 equiv) was added to a solution of **3** (101.0 mg, 0.1113 mmol) in 7 mL of toluene. The suspension was stirred for a period of 2.5 h at a temperature of 110 °C. Then, the formed pale-yellow precipitate was separated by filtration, washed three times with 5 mL portions of Et_2O, and dried. The raw product (115.8 mg, 89%, 0.0985 mmol) was recrystallized from a CH_2Cl_2/Et_2O mixture. $\mathbf{3}(CuCN)_3{\cdot}2CH_2Cl_2$, $C_{53}H_{82}N_{21}Cu_3Cl_4$ (1345.81): calcd C 47.30, H 6.14, N 21.86; C 47.40, H 6.28, N 22.05. HR-ESI$^+$ (MeOH): m/z = 1176.47175 [$\mathbf{3}(CuCN)_3$ + H]$^+$, 3.0%, calcd 1176.47065; 1149.46224 [$\mathbf{3}(CuCN)_2$ + Cu]$^+$, 4.3%, calcd 1149.45972; 1085.54057 [$\mathbf{3}(CuCN)_2$ + H]$^+$, 48.4%, calcd 1085.53886; 1060.53016 [$\mathbf{3}(CuCN)$ + Cu]$^+$, 20.0%, calcd 1060.52737; 996.60697 [$\mathbf{3}(CuCN)$ + H]$^+$, 79.8%, calcd 996.60619; 530.76771 [$\mathbf{3}(CuCN)$ + Cu + H]$^{2+}$, 28.9%, calcd 530.76760; 498.80724 [$\mathbf{3}(CuCN)$ + 2H]$^{2+}$, 100.0%, calcd 498.80701. ^{1}H NMR (600.13 MHz, CD_2Cl_2): δ = 7.23 (s, 6H, H_{arom}), 2.93 (s, 72H, CH_3) ppm. $^{13}C\{^1H\}$ NMR (150.90 MHz, CD_2Cl_2), HSQC, HMBC: δ = 163.96 (N═C), 141.95 (C_{arom}), 124.45 (C_{arom}), 110.94 (CH_{arom}), 40.69 (CH_3) ppm. IR (CsI): ν = 3065 (w), 3002 (w), 2935 (m), 2874 (m), 2796 (w), 2124 (w, shoulder), 2104 (m), 1516 (s), 1489 (s), 1467 (s), 1420 (s), 1392 (s), 1333 (m), 1313 (m), 1274 (m), 1231 (m), 1188 (m), 1155 (s), 1107 (w), 1063 (m), 1034 (s), 1000 (s), 917 (m), 869 (s), 849 (m), 809 (s), 756 (m), 728 (m), 703 (m), 664 (w), 630 (m), 601 (w) cm^{-1}. IR ($CHCl_3$ solution): ν = 3000 (m), 2945 (w), 2891 (w), 2870 (w), 2798 (w), 2135 (w), 2100 (m), 1531 (s), 1489 (s), 1468 (m), 1420 (s), 1407 (w), 1393 (s), 1335 (w), 1311 (w), 1273 (w), 1244 (w), 1154 (m), 1141 (m), 1106 (w), 1063 (w), 1034 (m), 1000 (m) cm^{-1}. UV/vis (CH_2Cl_2, c = 2.8913 × 10^{-5} mol/L, d = 0.5 cm): λ (ε, M^{-1} cm^{-1}) = 397 (38643), 379 (45428), 340 (71506), 311 (55128), ca. 228 (67249) nm. Crystal data for $\mathbf{3}(CuCN)_3{\cdot}4.6CH_2Cl_2$, $C_{53.30}H_{82.60}Cl_{4.60}Cu_3N_{21}$: M_r = 1377.69, 0.35 × 0.20 × 0.15 mm^3, triclinic, space group $P\bar{1}$, a = 15.275(3) Å, b = 15.419(3) Å, c = 17.478(4) Å, α = 104.69(3)°, β = 108.99(3)°, γ = 109.05(3)°, V = 3368.1(12) $Å^3$, Z = 2, d_{calc} = 1.358 $Mg{\cdot}m^{-3}$, Mo Kα radiation (graphite-monochromated, λ = 0.71073 Å), T = 100 K, θ_{range} 2.17−29.10°. Reflns measd 33156, indep 17928, R_{int} = 0.0380. Final R indices [$I > 2\sigma(I)$]: R1 = 0.0548, wR2 = 0.1463.

Synthesis of 3(CuCl)$_3$. **3** (35.6 mg, 0.0394 mmol) and CuCl (11.7 mg, 0.1182 mmol, 3 equiv) were suspended in 6 mL of toluene and stirred for a period of 3 h at 110 °C. A beige precipitate formed that was separated by filtration, washed first two times with 3 mL portions of toluene and then three times with 3 mL portions of Et_2O, and finally dried. The raw product, obtained in this way in the form of a yellow solid in 70% yield (22.4 mg, 0.0277 mmol), was recrystallized from a CH_2Cl_2/Et_2O mixture. $\mathbf{3}(CuCl)_3{\cdot}CH_2Cl_2$, $C_{49}H_{80}N_{18}Cu_3Cl_5$ (1289.18): calcd C 45.65, H 6.25, N 19.56; found C 45.66, H 6.31, N 19.84. HR-ESI$^+$ (MeCN): m/z = 1241.33935 [$\mathbf{3}(CuCl)_3$ + Cl + 2H]$^+$, 2.1%, calcd 1241.33910; 1203.336608 [$\mathbf{3}(CuCl)_3$ + H]$^+$, 1.3%, calcd 1203.36537; 1169.41784 [$\mathbf{3}(CuCl)_2$ + Cu + 2H]$^+$, 2.4%, calcd 1169.40628; 1141.44425 [$\mathbf{3}(CuCl)_2$ + Cl + 2H]$^+$, 5.8%, calcd 1141.44536; 1105.46783 [$\mathbf{3}(CuCl)_2$ + H]$^+$, 8.2%, calcd 1105.46891; 1043.54575 [$\mathbf{3}(CuCl)$ + Cl + 2H]$^+$, 12.0%, calcd 1043.54725; 1005.57172 [$\mathbf{3}(CuCl)$ + H]$^+$, 8.7%, calcd 1005.57196; 907.67329 [**3** + H]$^+$, 14.4%, calcd 907.67351; 536.26336 [$\mathbf{3}(CuCl)$ + Cu + 3H]$^{2+}$, 6.4%, calcd 536.25802; 522.27653 [$\mathbf{3}(CuCl)$ + Cl + 3H]$^{2+}$, 14.8%, calcd 522.27754; 503.28948 [$\mathbf{3}(CuCl)$ + 2H]$^{2+}$, 21.3%, calcd 503.28989; 454.34015 [**3** + 2H]$^{2+}$, 100.0%, calcd 454.34067; 303.22929 [**3** + 3H]$^{3+}$, 32.9%, calcd 303.22972. ^{1}H NMR (600.13 MHz, CD_2Cl_2): δ = 7.26 (s, 6H, H_{arom}), 2.91 (s, 72H, CH_3) ppm. $^{13}C\{^1H\}$ NMR (150.90 MHz, CD_2Cl_2), HSQC, HMBC: δ = 163.28 (N═C), 141.56 (C_{arom}), 124.42 (C_{arom}), 111.31 (CH_{arom}), 40.50 (CH_3) ppm. IR (CsI): ν = 3066 (w), 3004 (w), 2936 (m), 2880 (m), 2797 (w), 1629 (m, shoulder), 1572 (s), 1522 (s), 1490 (s), 1466 (s), 1419 (s), 1402 (s), 1331 (m), 1315 (m), 1275 (m), 1232 (m), 1188 (m), 1155 (s), 1106 (w), 1064 (m), 1035 (s), 1002 (m), 926 (w), 915 (w), 866 (s), 845 (m), 826 (m), 805 (m), 755 (w), 737 (m), 726 (m), 702 (m), 662 (w), 630 (m), 602 (w) cm^{-1}. UV/vis (CH_2Cl_2, c = 2.4202 × 10^{-5} mol/L, d = 0.5 cm): λ (ε, M^{-1} cm^{-1}) = 397 (47237), 377 (56400), 339 (86659), 311 (61938), 237 (57365) nm. Crystal data for $\mathbf{3}(CuCl)_3{\cdot}1.7CH_2Cl_2$, $C_{49.70}H_{81.40}Cl_{6.40}Cu_3N_{18}$: M_r = 1348.63, 0.40 × 0.30 × 0.22 mm^3, monoclinic, space group $C2/c$, a = 30.408(6) Å, b = 17.433(4) Å, c = 29.641(6) Å, β = 120.29(3)°, V = 13568(5) $Å^3$, Z = 8, d_{calc} = 1.320 $Mg{\cdot}m^{-3}$, Mo Kα radiation (graphite-monochromated, λ = 0.71073 Å), T = 100 K, θ_{range} 2.35−27.53°. Reflns measd 15539, indep 15539, R_{int} = 0.0259. Final R indices [$I > 2\sigma(I)$]: R1 = 0.0570, wR2 = 0.1746.

Synthesis of 3(CuBr)$_3$. A solution of **3** (47.9 mg, 0.0527 mmol) in 6 mL of toluene was added to a Schlenk flask containing CuI (22.7 mg, 0.1582 mmol, 3 equiv). The suspension was stirred in boiling toluene for a period of 2.5 h. The pale-brown-colored precipitate was separated by filtration, washed two times with 3 mL portions of toluene and then three times with 3 mL portions of Et_2O, and subsequently dried. The product was isolated as a yellow solid in a yield of 66% (46.3 mg, 0.0346 mmol). $C_{48}H_{78}N_{18}Cu_3Br_3$ (1337.60): calcd C 43.10, H 5.88, N 18.85; found C 42.45, H 5.67, N 18.81. HR-ESI$^+$ (CH_2Cl_2): m/z = 1336.21038 [$\mathbf{3}(CuBr)_3$]$^+$, 3.7%, calcd 1336.20625; 1257.29367 [$\mathbf{3}(CuBr)_2$ + Cu]$^+$, 40.0%, calcd 1257.28819; 1195.36980 [$\mathbf{3}(CuBr)_2$ + H]$^+$, 100.0%, calcd 1195.36656; 1051.52683 [$\mathbf{3}(CuBr)$ + H]$^+$, 3.5%, calcd 1051.52028; 557.22727 [$\mathbf{3}(CuBr)$ + Cu + H]$^{2+}$, 12.2%, calcd 557.22487; 526.26615 [$\mathbf{3}(CuBr)_2$ + 2H]$^{2+}$, 8.8%, calcd 526.26405. ^{1}H NMR (600.13 MHz, CD_2Cl_2): δ = 7.27 (s, 6H, H_{arom}), 2.93 (s, 72H, CH_3) ppm. $^{13}C\{^1H\}$ NMR (150.90 MHz, CD_2Cl_2), HSQC, HMBC: δ = 163.31 (C═N), 141.60 (C_{arom}), 124.50 (C_{arom}), 111.27 (CH_{arom}), 40.45 (CH_3) ppm. IR (CsI): ν = 3066 (w), 3001 (w), 2930 (m), 2872 (m), 2793 (w), 1567 (s, shoulder), 1533 (s), 1520 (s), 1491 (s), 1466 (s), 1417 (s), 1395 (s), 1388 (s), 1332 (s), 1315 (m), 1275 (m), 1227 (m), 1191 (w), 1152 (s), 1105 (w), 1064 (w), 1033 (s), 1001 (s), 970 (w), 918 (w), 861 (m), 848 (m), 815 (m), 805 (m), 755 (w), 737 (w), 725 (m), 699 (m), 630 (w), 601 (w) cm^{-1}. UV/vis (CH_2Cl_2, c = 1.8690 × 10^{-5} mol/L, d = 0.5 cm): λ (ε, M^{-1} cm^{-1}) = 397 (50691), 377 (60644), 341 (92132), 310 (60925), 231 (66648) nm. Crystal data for $\mathbf{3}(CuBr)_3{\cdot}2.8CH_2Cl_2$, $C_{50.80}H_{83.60}Br_3Cl_{5.60}Cu_3N_{18}$, M_r = 1575.43, 0.40 × 0.30 × 0.25 mm^3, triclinic, space group $P\bar{1}$, a = 15.234(3) Å, b = 15.525(3) Å, c = 17.541(4) Å, α = 109.20(3), β = 104.86(3)°, γ = 109.32(3), V = 3372.3(12) $Å^3$, Z = 2, d_{calc} = 1.552 $Mg{\cdot}m^{-3}$, Mo Kα radiation (graphite-monochromated, λ = 0.71073 Å), T = 100 K, θ_{range} 2.48−27.62°. Reflns measd 62325, indep 15523, R_{int} = 0.1014. Final R indices [$I > 2\sigma(I)$]: R1 = 0.0718, wR2 = 0.1888.

Synthesis of 3(CuI)$_3$. A solution of compound **3** (50.0 mg, 0.0551 mmol) in 4 mL of toluene was added to a suspension of CuI (31.5 mg, 0.1653 mmol, 3 equiv) in 2 mL of toluene. The reaction mixture was stirred for a period of 3 h at a temperature of 110 °C. The pale-yellow precipitate was separated from the mixture by filtration, washed first two times with 2 mL portions of toluene and then three times with 2 mL portions of Et_2O, and finally dried. A yield of 52.0 mg (64%, 0.0352 mmol) was obtained in the form of a yellow solid. $C_{48}H_{78}N_{18}Cu_3I_3$ (1478.60): calcd C 38.99, H 5.32, N 17.05; found C 38.82, H 4.86, N 17.20. HR-ESI$^+$ (CH_2Cl_2, MeOH): m/z = 1289.34489 [$\mathbf{3}(CuI)_2$ + H]$^+$, 6.4%, calcd 1289.34101; 1225.42371 [$\mathbf{3}(CuI)$ + I + 2H]$^+$, 9.4%, calcd 1225.41987; 1097.50696 [$\mathbf{3}(CuI)$ + H]$^+$, 8.3%, calcd 1097.50758; 549.25753 [$\mathbf{3}(CuI)$ + 2H]$^{2+}$, 100.0%, calcd 549.25770. ^{1}H NMR (600.13 MHz, CD_2Cl_2): δ = 7.25 (s, 6H, H_{arom}), 2.96 (s, 72H, CH_3) ppm. $^{13}C\{^1H\}$ NMR (150.90 MHz, CD_2Cl_2), HSQC, HMBC: δ = 163.60 (N═C), 141.89 (C_{arom}), 124.31 (C_{arom}), 111.14 (CH_{arom}), 40.63 (CH_3) ppm. IR (CsI): ν = 3065 (w), 3004 (w), 2936 (w), 2873 (w), 2793 (w), 1566 (s), 1534 (s), 1522 (s), 1490 (s), 1466 (s), 1418 (s), 1391 (s), 1333 (m), 1314 (m), 1274 (w), 1232 (m), 1190 (w), 1154 (s), 1106 (w), 1063 (w), 1033 (m), 1001 (m), 925 (w), 917 (w), 867 (w), 847 (w), 813 (w), 804 (w), 754 (w), 738 (w), 725 (w), 701 (w), 627 (w), 602 (w), 504 (w) cm^{-1}. UV/vis (CH_2Cl_2, c = 1.8125 × 10^{-5} mol/L, d = 0.5 cm): λ (ε, M^{-1} cm^{-1}) =

dx.doi.org/10.1021/ic501482u | Inorg. Chem. 2014, 53, 9876−9896

399 (40375), 380 (47672), 342 (75425), 313 (50722), 237 (60425) nm.

Synthesis of 3(CuCl$_2$)$_3$. A solution of **3** (87.5 mg, 0.0964 mmol) in 4 mL of CH_3CN was added to a solution of $CuCl_2$ (37.6 mg, 0.2797 mmol, 2.9 equiv) in 4 mL of CH_3CN. The deep-green-colored reaction mixture was stirred at room temperature for a period of 1 h. Then, the solvent was removed in vacuo, and the green solid was washed first two times with 4 mL portions of toluene and then three times with 4 mL portions of Et_2O. After drying, the product was obtained as a green solid in a yield of 82% (103.1 mg, 0.0787 mmol). The product was recrystallized from a CH_2Cl_2/C_6H_{14} (hexane) mixture. $C_{48}H_{78}N_{18}Cu_3Cl_6$ (1310.61): calcd C 43.99, H 6.00, N 19.24; found C 43.72, H 5.94, N 18.79. HR-ESI$^+$ (CH_3CN): m/z = 1309.26450 [**3**(CuCl$_2$)$_3$]$^+$, 2.4%, calcd 1309.26348; 1274.29475 [**3**(CuCl$_2$)$_2$(CuCl)]$^+$, 3.3%, calcd 1274.29482; 1174.39875 [**3**(CuCl$_2$)$_2$]$^+$, 6.7%, calcd 1174.39840; 1139.43018 [**3**(CuCl$_2$)(CuCl)]$^+$, 14.8%, calcd 1139.42971; 1039.53460 [**3**(CuCl$_2$)]$^+$, 2.4%, calcd 1039.53299; 1026.33537 [**3**(CuCl$_2$)(CuCl) + H − NC(NMe$_2$)$_2$]$^{2+}$, 4.8%, calcd 1026.33429; 620.16706 [**3**(CuCl$_2$)(CuCl)$_2$ + H]$^{2+}$, 18.7%, calcd 620.16701; 587.19930 [**3**(CuCl$_2$)$_2$]$^{2+}$, 17.4%, calcd 620.19920, 552.23051 [**3**(CuCl)$_2$]$^{2+}$, 38.9%, calcd 552.23054, 520.76547 [**3**(CuCl$_2$)]$^{2+}$, 34.6%, calcd 520.76580, 502.78619 [**3**(CuCl) + H]$^{2+}$, 67.9%, calcd 502.78598. IR (CsI): ν = 3011 (w), 2932 (m), 2893 (w), 2870 (w), 2795 (w), 1624 (w, shoulder), 1577 (s), 1515 (s), 1491 (s), 1460 (m), 1418 (s), 1400 (s), 1329 (m), 1319 (m), 1277 (m), 1231 (m), 1189 (w), 1163 (m), 1140 (w), 1105 (w), 1064 (m), 1041 (m), 1006 (m), 924 (w), 912 (w), 886 (w), 865 (m), 824 (m), 806 (w), 766 (w), 737 (w), 721 (w), 701 (w), 668 (w), 665 (w), 632 (w), 628 (w) cm^{-1}. Evans NMR (CD_2Cl_2): $\Delta\nu$ = 28.225 Hz, χ_{Mol} = 5.1478 × 10^{-3} cm^3/mol, μ_{eff} = 3.53 μ_B, [μ_{SO}(3e$^-$) = 3.87 μ_B]. UV/vis (CH_2Cl_2, c = 1.9228 × 10^{-5} mol/L, d = 0.5 cm): λ (ε, M^{-1} cm^{-1}) = 1132 (832), 688 (1486), ca. 490 (1551, shoulder), 397 (53500), 376 (63760), 341 (97461), 307 (60956), 240 (48683) nm. Crystal data for **3**(CuCl$_2$)$_3$·3CH$_2$Cl$_2$, $C_{51}H_{84}Cl_{12}Cu_3N_{18}$, M_r = 1565.38, 0.50 × 0.50 × 0.45 mm^3, monoclinic, space group $C2/c$, a = 28.949(6) Å, b = 17.537(4) Å, c = 15.714(3) Å, β = 96.85(3)°, V = 7921(3) Å^3, Z = 4, d_{calc} = 1.313 Mg·m^{-3}, Mo Kα radiation (graphite-monochromated, λ = 0.71073 Å), T = 100 K, θ_{range} 2.63−27.49°. Reflns measd 17404, indep 8979, R_{int} = 0.0207. Final R indices [$I > 2\sigma(I)$]: R1 = 0.0625, wR2 = 0.1835.

Synthesis of 3(CuBr$_2$)$_3$. Compound **3** (50.0 mg, 0.0551 mmol) was dissolved in 3 mL of CH_3CN, and the solution was added to a solution of $CuBr_2$ (36.9 mg, 0.1653 mmol, 3 equiv) in 3 mL of CH_3CN. The initially shiny deep-green-colored solution turned olive green-brown, and a dark solid precipitate formed after some time. The reaction mixture was stirred at room temperature for a period of 1.5 h, and subsequently, the solvent was removed under a vacuum. The solid was washed three times with 2 mL portions of Et_2O and dried. The product was isolated as an olive-green solid in a yield of 96% (83.0 mg, 0.0526 mmol). $C_{48}H_{78}N_{18}Cu_3Br_6$ (1577.32): calcd C 36.55, H 4.98, N 15.98; obsd C 36.42, H 4.75, N 15.81. FAB$^+$: m/z = 1576.9 [**3**(CuBr$_2$)$_3$]$^+$, 5.5%; 1498.1 [**3**(CuBr$_2$)$_2$ + CuBr]$^+$, 10.0%; 1417.2 [**3**(CuBr$_2$)$_2$ + Cu]$^+$, 12.0%; 1355.2 [**3**(CuBr$_2$)$_2$ + H]$^+$, 10.5%; 1273.3 [**3**(CuBr$_2$) + CuBr]$^+$, 22.5%; 1194.4 [**3**(CuBr$_2$) + Cu]$^+$, 32.0%; 1050.5 [**3**(CuBr)]$^+$, 24.0%; 906.6 [**3**]$^+$, 74.0%. HR-FAB$^+$: m/z = 1273.2692 [**3**(CuBr$_2$) + CuBr]$^+$, 74.0%, calcd 1273.2768; 1194.3564 [**3**(CuBr$_2$) + Cu]$^+$, 100.0%, calcd 1194.3588. IR (CsI): ν = 3010 (w), 2930 (m), 2895 (w), 2870 (w), 2796 (w), 1624 (w, shoulder), 1574 (s), 1513 (s), 1490 (s), 1459 (s), 1417 (s), 1399 (s), 1327 (m), 1277 (m), 1232 (m), 1188 (w), 1162 (m), 1138 (m), 1103 (w), 1063 (m), 1040 (m), 1006 (m), 923 (w), 911 (w), 864 (m), 823 (m), 804 (w), 762 (w), 737 (w), 719 (w), 702 (w), 662 (w), 628 (w), 502 (w) cm^{-1}. UV/vis (CH_2Cl_2, c = 1.7371 × 10^{-5} mol/L, d = 0.5 cm): λ (ε, M^{-1} cm^{-1}) = 1152 (1097), 754 (2132), ca. 490 (3519, shoulder), 399 (53447), 377 (64169), 342 (93861), 310 (55362), 240 (46440) nm.

Synthesis of 3(CuI$_2$)$_3$. A solution of I_2 (25.7 mg, 0.1014 mmol) in 2.5 mL of CH_3CN was added to a suspension of **3**(CuI)$_3$ (50.0 mg, 0.0338 mmol) in 7 mL of CH_3CN. The dark-brown reaction mixture was stirred at room temperature for a period of 1.5 h and then filtered. The black residue (40.0 mg, 0.0215 mmol, 64%) was dissolved in CH_2Cl_2 and recrystallized by slow diffusion of Et_2O and $CHCl_3$ into the solution. $C_{48}H_{78}N_{18}Cu_3I_6$ (1859.32): calcd C 31.01, H 4.23, N 13.56; found C 30.45, H 4.35, N 13.22. HR-ESI$^+$ (CH_2Cl_2 + MeOH): m/z = 1287.34364 [**3**(CuI)$_2$ + H]$^+$, 7.6%, calcd 1287.34165; 1197.40610 [**3**(CuI)(CuCl) + H]$^+$, 2.9%, calcd 1197.40486; 1097.50971 [**3**(CuI) + H]$^+$, 3.4%, calcd 1097.50758; 643.67160 [**3**(CuI)$_2$ + H]$^{2+}$, 43.6%, calcd 643.67082; 598.70275 [**3**(CuI)(CuCl) + H]$^{2+}$, 20.6%, calcd 598.70243; 580.21949 [**3**(CuI) + Cu + H]$^{2+}$, 8.2%, calcd 580.21859; 549.25793 [**3**(CuI) + 2H]$^{2+}$, 100.0%, calcd 549.25770. IR (CsI): ν = 3006 (w), 2929 (w), 2889 (w), 2863 (w), 2790 (w), 1617 (w, sholder), 1570 (s), 1513 (s), 1489 (s), 1465 (m), 1457 (m), 1415 (s), 1399 (s), 1327 (m), 1321 (m), 1274 (w), 1231 (m), 1222 (m), 1189 (w), 1161 (s), 1139 (w), 1104 (w), 1062 (w), 1040 (m), 1005 (m), 923 (w), 911 (w), 862 (m), 821 (m), 803 (w), 763 (w), 735 (w), 720 (w), 701 (w), 668 (w), 626 (w), 503 (w) cm^{-1}. UV/vis (CH_2Cl_2, c = 1.3123 × 10^{-5} mol/L, d = 0.5 cm): λ (ε, M^{-1} cm^{-1}) = 911 (4281), 667 (2606), ca. 497 (8106, shoulder), 400 (53747), 380 (63305), 345 (88618), 310 (43963), 234 (58719, shoulder) nm. Crystal data for **3**(CuI$_2$)$_3$·4.45CHCl$_3$·0.8CH$_2$Cl$_2$, $C_{53.25}H_{84.05}Cl_{14.95}Cu_3I_6N_{18}$: M_r = 2458.43, 0.30 × 0.20 × 0.15 mm^3, monoclinic, space group $P2_1/c$, a = 28.958(6) Å, b = 17.326(4) Å, c = 20.477(4) Å, β = 107.67(3)°, V = 9789(3) Å^3, Z = 4, d_{calc} = 1.668 Mg·m^{-3}, Mo Kα radiation (graphite-monochromated, λ = 0.71073 Å), T = 100 K, θ_{range} 0.74−27.70°. Reflns measd 155781, indep 22583, R_{int} = 0.0668. Final R indices [$I > 2\sigma(I)$]: R1 = 0.0612, wR2 = 0.1769.

Synthesis of 3(NiCl$_2$)$_3$. A solution of **3** (32.6 mg, 0.0359 mmol) in 3 mL of CH_2Cl_2 was cooled to −78 °C and then added to a suspension of NiCl$_2$·dme (22.8 mg, 0.1041 mmol, 2.9 equiv) in 3 mL of CH_2Cl_2 that had also been cooled to −78 °C. Then, the reaction mixture was slowly allowed to warm to room temperature overnight. After removal of the solvent under a vacuum, the red-brown residue was washed three times with 3 mL portions of C_6H_{14} (hexane) and subsequently dried. The product was obtained in a yield of 38.2 mg (0.0295 mmol, 82%). It was recrystallized from CH_2Cl_2/C_6H_{14}. $C_{48}H_{78}N_{18}Ni_3Cl_6$ (1296.05): calcd C 44.48, H 6.07, N 19.45; found C 44.00, H 6.29, N 18.01. LIFDI (CH_2Cl_2): m/z = 1259.3 [**3**(NiCl$_2$)$_3$ − Cl]$^+$, 19%; 1129.5 [[**3**(NiCl$_2$)$_2$ − Cl]$^+$, 30%; 1037.5 [[**3**(NiCl$_2$) + H]$^+$, 53%; 999.4 [[**3**(NiCl$_2$) − Cl]$^+$, 43%; 907.6 [**3** + H]$^+$, 100%. ^{1}H NMR (200 MHz, CD_2Cl_2): δ = 45.85 (s, CH_3), 9.17 (s, H_{arom}). IR (CsI): ν = 3009 (w), 2940 (m), 2893 (w), 2800 (w), 1558 (s), 1522 (s), 1491 (s), 1466 (m), 1420 (s), 1410 (s), 1398 (s), 1333 (m), 1314 (m), 1273 (w), 1238 (m), 1188 (w), 1161 (m), 1142 (m), 1109 (w), 1065 (w), 1040 (m), 1005 (w), 986 (w), 914 (w), 864 (m), 822 (m), 762 (w), 737 (w), 723 (w), 708 (w), 669 (w), 635 (w), 602 (w) cm^{-1}. UV/vis (CH_3CN, c = 1.88 × 10^{-5} mol/L, d = 1 cm): λ (ε, M^{-1} cm^{-1}) = 684 (274), 580 (618), 512 (1350), ca. 453 (3691, shoulder), 365 (49395), 331 (83446), 235 (51455) nm. Crystal data for **3**(NiCl$_2$)$_3$·4CH$_2$Cl$_2$, $C_{52}H_{86}Cl_{14}N_{18}Ni_3$, M_r = 1635.82, 0.40 × 0.30 × 0.30 mm^3, triclinic, space group $P\bar{1}$, a = 16.234(3) Å, b = 17.325(4) Å, c = 17.430(4) Å, α = 93.05(3)°, β = 106.58(3)°, γ = 117.31(3)°, V = 4076.1(14) Å^3, Z = 2, d_{calc} = 1.333 Mg·m^{-3}, Mo Kα radiation (graphite-monochromated, λ = 0.71073 Å), T = 100 K, θ_{range} 2.03−28.50°. Reflns measd 69667, indep 20626, R_{int} = 0.0556. Final R indices [$I > 2\sigma(I)$]: R1 = 0.0917, wR2 = 0.2696.

Synthesis of 3(NiBr$_2$)$_3$. A solution of **3** (100.0 mg, 0.1102 mmol) in 6 mL of CH_2Cl_2 was cooled to −78 °C and then added to a suspension of NiBr$_2$·dme (100.9 mg, 0.3269 mmol, 2.97 equiv) in 5 mL of CH_2Cl_2, also kept at a temperature of −78 °C. Then, the reaction mixture was slowly allowed to warm to room temperature overnight. The red-brown suspension was filtered, and the solvent was removed from the filtrate under a vacuum. The brown solid was washed three times with 4 mL portions of C_6H_{14} and then dried. The product was obtained in a yield of 132.0 mg (0.0845 mmol, 77%). $C_{48}H_{78}N_{18}Ni_3Br_6$ (1562.98): calcd C 36.89, H 5.03, N 16.13; found C 36.83, H 5.14, N 15.71. ^{1}H NMR (200 MHz, CD_2Cl_2): δ = 46.28 (s, CH_3), 9.94 (s, H_{arom}). IR (CsI): ν = 3007 (w), 2934 (m), 2887 (w), 2799 (w), 1552 (s), 1522 (s), 1491 (s), 1466 (m), 1418 (s), 1410 (s), 1398 (s), 1333 (m), 1317 (m), 1277 (m), 1233 (m), 1188 (w), 1161 (m), 1142 (m), 1107 (w), 1063 (w), 1040 (m), 1007 (m), 916 (w), 864 (m), 824 (m), 802 (w), 760 (w), 737 (w), 723 (w), 704 (w), 669

dx.doi.org/10.1021/ic501482u | Inorg. Chem. 2014, 53, 9876−9896

(w), 633 (w), 602 (w) cm^{-1}. UV/vis (CH_3CN, $c = 1.30 \times 10^{-5}$ mol/L, d = 1 cm): λ (ε, M^{-1} cm^{-1}) = ca. 708 (296), ca. 607 (987), ca. 539 (630), ca. 466 (3317), 364 (51868), 332 (84890) nm.

Synthesis of 3(CoCl$_2$)$_3$. A solution of ligand **3** (54.9 mg, 0.0606 mmol) in 3.0 mL of CH_3CN was added to a solution of $CoCl_2$ (22.8 mg, 0.1756 mmol, 2.9 equiv) in 2.0 mL of CH_3CN. The deep-blue-colored solution was stirred at room temperature for a period of 2 h, during which time a blue precipitate formed. Then, the solvent was removed under a vacuum, and the solid was washed first two times with 3 mL portions of toluene and then two times with 3 mL portions of Et_2O. The product was obtained in a yield 57.2 mg (0.0441 mmol, 73%). It was recrystallized from CH_2Cl_2/Et_2O. $C_{48}H_{78}N_{18}Co_3Cl_6$ (1296.77): calcd C 44.46, H 6.06, N 19.44, obsd C 44.20, H 6.14, N 19.12. HR-ESI$^+$ (CH_3CN): m/z = 1260.30662 [**3**$(CoCl_2)_3 - Cl]^+$, 21.9%, calcd 1260.30740; 1167.41237 [**3**$(CoCl_2)_2 + H]^+$, 23.6%, calcd 1167.41336; 612.66889 [**3**$(CoCl_2)_3 - 2Cl]^{2+}$, 29.1%, calcd 612.66935; 565.22298 [**3**$(CoCl_2)$ + Cl + H$]^{2+}$, 100.0%, calcd 565.22323. ^{1}H NMR (200 MHz, CD_2Cl_2): δ = 31.06 (s, CH_3), 22.19 (s, H_{arom}). IR (CsI): ν = 3010 (w), 2939 (w), 2800 (w), 1558 (s), 1521 (s), 1491 (m), 1495 (m), 1420 (s), 1407 (s), 1399 (s), 1331 (m), 1314 (m), 1270 (m), 1239 (s), 1188 (w), 1160 (m), 1141 (m), 1108 (w), 1064 (w), 1039 (m), 1004 (m), 985 (m), 913 (w), 863 (m), 820 (m), 724 (w), 708 (w), 665 (w) cm^{-1}. UV/vis (CH_3CN, $c = 1.59 \times 10^{-5}$ mol/L, d = 1 cm): λ (ε, M^{-1} cm^{-1}) = 664 (1195), 622 (1066), 568 (824), 550 (786), 373 (64906), 331 (103836) nm. Crystal structure measured (see Supporting Information).

Synthesis of 3(AgCN)$_3$. **3** (40 mg, 0.0441 mmol) and AgCN (17.7 mg, 0.1322 mmol, 3 equiv) were suspended in 5 mL of toluene. The reaction mixture was stirred in refluxing toluene for a period of 2.5 h. Then, the pale-yellow-colored precipitate was separated by filtration, washed two times with 2 mL portions of toluene and three times with 2 mL portions of Et_2O, and subsequently dried. The raw product (46.4 mg, 0.0354 mmol, 80%) was finally recrystallized from a CH_2Cl_2/Et_2O mixture. **3**$(AgCN)_3 \cdot CH_2Cl_2$, $C_{52}H_{80}N_{21}Ag_3Cl_2$ (1393.84): calcd C 44.81, H 5.79, N 21.10; found C 44.71, H 5.79, N 21.45. HR-ESI$^+$ (MeOH): m/z = 1308.40301 [**3**$(AgCN)_3$ + H$]^+$, 9.8%, calcd 1308.39805; 1281.39241 [**3**$(AgCN)_3$ − CN$]^+$, 10.6%, calcd 1281.387136; 1175.49601 [**3**$(AgCN)_2$ + H$]^+$, 27.2%, calcd 1175.49003; 1148.48384 [**3**$(AgCN)_2$ − CN$]^+$, 39.0%, calcd 1148.479114; 1042.58486 [**3**$(AgCN)$ + H$]^+$, 100.0%, calcd 1042.582270; 907.67809 [**3** + H$]^+$, 9.4%, calcd 907.6735; 520.79592 [**3**$(AgCN)$ + 2H$]^{2+}$, 19.8%, calcd 520.79475. ^{1}H NMR (600.13 MHz, CD_2Cl_2): δ = 7.20 (s, 6H, H_{arom}), 2.86 (s, 72H, CH_3) ppm. $^{13}C\{^1H\}$ NMR (150.90 MHz, CD_2Cl_2), HSQC, HMBC: δ = 164.08 (N═C), 141.28 (C_{arom}), 124.59 (C_{arom}), 112.34 (CH_{arom}), 40.63 (CH_3) ppm. IR (CsI): ν = 3061 (w), 3002 (w), 2932 (m), 2875 (m), 2795 (w), 2126 (m), 1533 (s), 1489 (s), 1469 (s), 1420 (s), 1390 (s), 1333 (m), 1306 (m), 1275 (m), 1232 (m), 1190 (w), 1152 (s), 1107 (w), 1062 (m), 1035 (s), 1000 (s), 920 (w), 869 (m), 846 (m), 801 (m), 753 (w), 737 (w), 726 (w), 702 (m), 668 (w), 661 (w), 629 (w), 600 (m) cm^{-1}. UV/vis (CH_2Cl_2, $c = 2.0475 \times 10^{-5}$ mol/L, d = 0.5 cm): λ (ε, M^{-1} cm^{-1}) = ca. 394 (37702), 374 (49211), 336 (84641), 308 (54546), ca. 231 (60829) nm. Crystal data for [**3**$(AgCN)_3$]·1.15CH_2Cl_2, $C_{52.15}H_{80.30}Ag_3Cl_{2.30}N_{21}$: M_r = 1406.62, 0.22 × 0.20 × 0.20 mm^3, triclinic, space group $P\bar{1}$, a = 17.508(4) Å, b = 17.583(4) Å, c = 25.244(5) Å, α = 79.13(3)°, β = 73.60(3)°, γ = 60.14(3)°, V = 6455(2) Å^3, Z = 4, d_{calc} = 1.447 Mg·m^{-3}, Mo Kα radiation (graphite-monochromated, λ = 0.71073 Å), T = 100 K, θ_{range} 0.84−27.57°. Reflns measd 56287, indep 29645, R_{int} = 0.0524. Final R indices [$I > 2\sigma(I)$]: R1 = 0.0683, wR2 = 0.1567.

Synthesis of [3(AgCl)$_3$]$_n$. Compound **3** (98 mg, 0.1080 mmol) was dissolved in 9 mL of toluene, and then AgCl (46.4 mg, 0.3240 mmol, 3 equiv) was added to this solution. The suspension was stirred in refluxing toluene for a period of 3 h. The flaky pale-yellow precipitate was separated by filtration. Then, it was washed five times with 4 mL portions of toluene and subsequently five times with 4 mL portions of Et_2O, and dried. The raw product (79.1 mg, 0.0592 mmol, 55%) was recrystallized from a CH_2Cl_2/Et_2O mixture. **3**$(AgCl)_3 \cdot CH_2Cl_2$, $C_{49}H_{80}N_{18}Ag_3Cl_5$ (1422.15): calcd C 41.38, H 5.67, N 17.73; found C 41.28, H 5.41, N 17.75. HR-ESI$^+$ (MeCN + MeOH): m/z = 1337.29419 [**3**$(AgCl)_3$ + H$]^+$, 0.8%, calcd 1337.28890; 1193.42227 [**3**$(AgCl)_2$ + H$]^+$, 4.5%, calcd 1193.420811; 1087.52383 [**3**$(AgCl)$ + Cl + 2H$]^+$, 10.3%, calcd 1087.52063; 1051.54752 [**3**$(AgCl)$ + H$]^+$, 5.6%, calcd 1051.547229; 907.67473 [**3** + H$]^+$, 8.9%, calcd 907.67351; 543.26629 [**3**$(AgCl)$ + Cl + 3H$]^{2+}$, 13.6%, calcd 543.26598; 526.27739 [**3**$(AgCl)$ + 2H$]^{2+}$, 100.0%, calcd 526.27753; 454.34068 [**3** + 2H$]^{2+}$, 43.0%, calcd 454.34067; 303.22945 [**3** + 3H$]^{3+}$, 23.6%, calcd 303.22972. ^{1}H NMR (600.13 MHz, CD_2Cl_2): δ = 7.25 (s, 6H, H_{arom}), 2.87 (s, 72H, CH_3) ppm. $^{13}C\{^1H\}$ NMR (150.90 MHz, CD_2Cl_2), HSQC, HMBC: δ = 163.65 (N═C), 140.90 (C_{arom}), 124.60 (C_{arom}), 112.65 (CH_{arom}), 40.58 (CH_3) ppm. IR (CsI): ν = 3061 (w), 3011 (w), 2995 (w), 2932 (m), 2869 (m), 2792 (w), 1564 (s), 1539 (s), 1519 (s), 1492 (s), 1468 (s), 1417 (s), 1396 (m), 1388 (s), 1333 (m), 1311 (m), 1275 (m), 1229 (s), 1194 (m), 1150 (s), 1105 (w), 1058 (m), 1034 (s), 1001 (s), 920 (w), 863 (m), 846 (m), 811 (m), 799 (m), 754 (w), 736 (w), 725 (m), 701 (m), 677 (w), 672 (w), 665 (w), 659 (w), 630 (w), 621 (w), 599 (m) cm^{-1}. UV/vis (CH_2Cl_2, $c = 1.5610 \times 10^{-5}$ mol/L, d = 0.5 cm): λ (ε, M^{-1} cm^{-1}) = ca. 394 (39327, shoulder), 374 (52493), 336 (91060), 308 (57287), 245 (46739) nm. Crystal data for [**3**$(AgCl)_3]_n$, $C_{48}H_{78}Ag_3Cl_3N_{18}$: M_r = 1337.24, 0.40 × 0.30 × 0.30 mm^3, triclinic, space group $P\bar{1}$, a = 13.099(3) Å, b = 17.406(4) Å, c = 17.403(4) Å, α = 61.82(3)°, β = 71.90(3)°, γ = 74.91(3)°, V = 3293.8(11) Å^3, Z = 2, d_{calc} = 1.348 Mg·m^{-3}, Mo Kα radiation (graphite-monochromated, λ = 0.71073 Å), T = 100 K, θ_{range} 2.26−27.52°. Reflns measd 27392, indep 14858, R_{int} = 0.0360. Final R indices [$I > 2\sigma(I)$]: R1 = 0.0855, wR2 = 0.2166.

Synthesis of [3(AgBr)$_3$]$_n$. AgBr (50.9 mg, 0.2711 mmol, 3 equiv) was added under exclusion of light to a solution of **3** (82.0 mg, 0.0904 mmol, 1 equiv) in 8 mL of toluene. The suspension was stirred overnight at a temperature of 110 °C. The pale-yellow-colored flaky precipitate was separated by filtration, washed first three times with 2 mL portions of toluene and then three times with 2 mL portions of Et_2O, and subsequently dried. The product was obtained in a yield of 122.8 mg (0.0835 mmol, 92%). It was recrystallized from CH_2Cl_2/Et_2O. $C_{48}H_{78}N_{18}Ag_3Br_3$ (1470.57): calcd C 39.20, H 5.35, N 17.14; found C 38.76, H 5.41, N 17.06. HR-ESI$^+$ (CH_3CN): m/z = 1445.16614 [**3** + $(AgBr)_2$ + 2Br + 3H$]^+$, 2.7%, calcd 1445.16601; 1175.42101 [**3**$(AgBr)$ + Br + 2H$]^+$, 3.5%, calcd 1175.42200; 1095.49507 [**3**$(AgBr)$ + H$]^+$, 4.2%, calcd 1095.49628; 907.67261 [**3** + H$]^+$, 19.9%, calcd 907.67351; 588.21390 [**3**$(AgBr)$ + Br + 3H$]^{2+}$, 19.5%, calcd 588.21491; 548.25119 **3**$(AgBr)$ + 2H$]^{2+}$, 24.1%, calcd 548.25201; 454.33998 [**3** + 2H$]^{2+}$, 100.0%, calcd 454.34067; 303.22913 [**3** + 3H$]^{3+}$, 95.9%, calcd 303.22972. FAB$^+$: m/z = 1390.4 [**3**$(AgBr)_2$ + Ag$]^+$, 1283.5 [**3**$(AgBr)_2$ + H$]^+$, 1203.5 [**3**$(AgBr)$ + Ag$]^+$, 1094.9 [**3**$(AgBr)$] $^+$, 1014.3 [**3** + Ag + H$]^+$. ^{1}H NMR (600.13 MHz, CD_2Cl_2): δ = 7.25 (s, 6H, H_{arom}), 2.87 (s, 72H, CH_3) ppm. $^{13}C\{^1H\}$ NMR (150.90 MHz, CD_2Cl_2), HSQC, HMBC: δ = 163.75 (N═C), 140.99 (C_{arom}), 124.58 (C_{arom}), 112.64 (CH_{arom}), 40.65 (CH_3) ppm. IR (CsI): ν = 3060 (w), 3000 (w), 2930 (m), 2880 (m), 2793 (w), 1539 (s), 1490 (s), 1466(s), 1457 (w), 1437 (w), 1420 (s), 1388 (s), 1334 (m), 1309 (m), 1275 (m), 1228 (m), 1192 (w), 1151 (s), 1106 (w), 1064 (m), 1034 (s), 1000 (s), 921 (w), 869 (m), 845 (m), 810 (m), 798 (m), 754 (w), 736 (m), 725 (m), 702 (m), 668 (w), 659 (w), 630 (w), 600 (m) cm^{-1}. UV/vis (CH_2Cl_2, $c = 1.7952 \times 10^{-5}$ mol/L, d = 0.5 cm): λ (ε, M^{-1} cm^{-1}) = 373 (51976), 335 (91534), 308 (59006), ca. 244 (56924) nm. Crystal data for [**3**$(AgBr)_3]_n \cdot 1.75CH_2Cl_2$, $C_{49.75}H_{81.50}Ag_3Br_3Cl_{3.50}N_{18}$: M_r = 1619.24, 0.30 × 0.28 × 0.25 mm^3, monoclinic, space group $P2_1/c$, a = 13.158(3) Å, b = 18.088(4) Å, c = 28.453(6) Å, β = 96.22(3)°, V = 6732(2) Å^3, Z = 4, d_{calc} = 1.598 Mg·m^{-3}, Mo Kα radiation (graphite-monochromated, λ = 0.71073 Å), T = 100 K, θ_{range} 2.11−28.69°. Reflns measd 34711, indep 17371, R_{int} = 0.0219. Final R indices [$I > 2\sigma(I)$]: R1 = 0.0515, wR2 = 0.1412.

Synthesis of [3(AgI)$_3$]$_n$. Compound **3** (58.3 mg, 0.0643 mmol) was dissolved in 7 mL of toluene, and AgI (45.3 mg, 0.1928 mmol, 3 equiv) was added to this solution. The suspension was stirred in boiling toluene for a period of 9 h. The pale-yellow precipitate was separated by filtration, washed first three times with 3 mL portions of toluene and then three times with 3 mL portions of Et_2O, and finally dried to give 73.5 mg of product (0.0456 mmol, 71%). Small crystals

dx.doi.org/10.1021/ic501482u | Inorg. Chem. 2014, 53, 9876−9896

were grown by slow diffusion of Et_2O into a CH_2Cl_2 solution. $C_{48}H_{78}N_{18}Ag_3I_3$ (1611.57): calcd C 35.77, H 4.88, N 15.64; found C 35.63, H 4.76, N 15.89. HR-ESI$^+$: m/z = 1143.48973 [**3**(AgI) + H]$^+$, 14.8%, calcd 1143.48363; 907.67443 [**3** + H]$^+$, 100.0%, calcd 907.67296. FAB$^+$: m/z = 907.7 [**3** + H]$^+$, 49.1%, 807.0 [**3**$(AgI)_3$ + 2H]$^{2+}$, 32.1%, 750.6 [**3**$(AgI)_2$ + I]$^{2+}$, 30.2%. ^{1}H NMR (200 MHz, CD_2Cl_2): δ = 7.27 (s, 6H, H_{arom}), 2.88 (s, 72H, CH_3) ppm. $^{13}C\{^1H\}$ NMR (150.90 MHz, CD_2Cl_2), HSQC, HMBC: δ = 163.71 (N=C), 112.43 (CH_{arom}), 40.82 (CH_3) ppm. IR (CsI): ν = 3059 (w), 2999 (w), 2929 (w), 2883 (m), 2794 (w), 1622 (m, shoulder), 1564 (s, shoulder), 1534 (s), 1487 (s), 1466(m), 1420 (s), 1388 (s), 1334 (w), 1302 (m), 1273 (w), 1233 (m), 1223 (m), 1189 (w), 1152 (s), 1106 (w), 1063 (m), 1033 (s), 997 (s), 920 (w), 869 (m), 841 (m), 805 (m), 796 (m), 752 (m), 736 (m), 726 (m), 704 (m), 667 (w), 631 (w), 599 (m) cm^{-1}. UV/vis (CH_2Cl_2, c = 1.7498 × 10^{-5} mol/L, d = 0.5 cm): λ (ε, M^{-1} cm^{-1}) = ca. 395 (38536, shoulder), 374 (51655), 336 (87982), 308 (54687), ca. 233 (64693, shoulder) nm. Crystal data for [**3**$(AgI)_3]_n$, $C_{48}H_{78}Ag_3I_3N_{18}$: M_r = 1611.59, 0.25 × 0.20 × 0.20 mm^3, monoclinic, space group $I2/m$, a = 14.89120(12) Å, b = 29.8096(3) Å, c = 18.5920(2) Å, β = 94.5880(9)°, V = 8226.56(15) Å^3, Z = 4, d_{calc} = 1.301 Mg·m^{-3}, Mo Kα radiation (graphite-monochromated, λ = 0.71073 Å), T = 100 K, θ_{range} 3.23−25.12°. Reflns measd 116949, indep 7491, R_{int} = 0.0390. Final R indices [$I > 2\sigma(I)$]: R1 = 0.0765, wR2 = 0.2310.

Crystal Structure Determination. Suitable crystals were removed directly from the mother liquor, immersed in perfluorinated polyether oil, and fixed on top of a glass capillary. Measurements were made with a Nonius-Kappa CCD diffractometer with a low-temperature unit using graphite-monochromated Mo Kα radiation. The temperature was set to 100 K. The data collected were processed using the standard Nonius software.[52] All calculations were performed using the SHELXT-PLUS software package. Structures were solved by direct methods with the SHELXS-97 program and refined with the SHELXL-97 program.[53,54] In the case of [**3**$(AgI)_3]_n$, attempts to find a satisfactory model for the solvent present in the structure were unsuccessful, and a diffuse solvent correction was applied to the intensity data of this compound using the SQUEEZE program of the Platon software suite.[55] Graphical handing of the structural data during solution and refinement was performed with XPMA.[56] Atomic coordinates and anisotropic thermal parameters of non-hydrogen atoms were refined by full-matrix least-squares calculations.

Details of the Quantum Chemical Calculations. DFT and TD-DFT calculations were carried out with the Gaussian 09[57] and TURBOMOLE[58] program packages. For all calculations, the B3LYP functional[59] was used, in combination with the 6-311G** basis set[60] for **3**, **3**$^{2+}$, **3**$^{4+}$, and **3**$^{6+}$ and with the def2-SV(P) basis set[61] for **3**$(CuI)_3$ and **3**$(CuI_2)_3$. Calculations with B3LYP/6-311G** and B3LYP/def2-SV(P) on the free ligand **3** gave very similar structures. The smaller def2-SV(P) basis set was chosen for the complexes with relatively large numbers of atoms leading to large computational times. Where applicable, the calculations on **3**$(CuI)_3$ and **3**$(CuI_2)_3$ were carried out with the resolution of the identity approximation for the coulomb integrals (RI-J)[58c] using the appropriate auxiliary SV(P) basis sets.[62] Additionally, the multipole accelerated resolution of the identity approximation (MARI-J) was employed.[58d] For the optimized structures of **3**$(CuI)_3$ and **3**$(CuI_2)_3$, TD-DFT calculations[58e] were performed. The excitation energies for 100 states were determined.

■ ASSOCIATED CONTENT

Ⓢ Supporting Information

Molecular structure of **4**; CV curves for **1** and **4** in CH_2Cl_2 solution; effects of the guanidino groups in **3** and **4** on the HOMO and LUMO energies of triphenylene; UV/vis spectra of **3**$(CuCN)_3$ and **3**$(AgCN)_3$ in CH_2Cl_2; details on the TD-DFT calculations of **3**$(CuI)_3$; molecular structure of **3**$(CuI_2)_3$; comparison of the UV/vis spectra of **3**$(CuCl_2)_3$, **3**$(CuBr_2)_3$, and **3**$(CuI_2)_3$ (in CH_2Cl_2 solution); validity check of the Lambert−Beer law for the complex **3**$(CuI_2)_3$ dissolved in CH_2Cl_2; details on the TD-DFT calculations of **3**$(CuI_2)_3$; CV curves for **3**$(CuCl_2)_3$ and **3**$(CuI_2)_3$; $\chi T-T$ curves as derived from SQUID measurements for **3**$(CuCl_2)_3$, **3**$(CuBr_2)_3$, **3**$(CuI_2)_3$, and **3**$(CoCl_2)_3$; molecular structure, UV/vis spectrum, and magnetization curves of **3**$(CoCl_2)_3$; structure of [**3**$(AgBr)_3]_n$; visualization of the voids in [**3**$(AgI)_3]_n$ using the program CrystalExplorer; details of the quantum chemical calculations (electronic energies; zero-point energy corrections; and x, y, and z coordinates for the optimized structures); and X-ray crystallographic data in cif format. This material is available free of charge via the Internet at http://pubs.acs.org. CCDC entries 999187 (**3**·6HCl), 999188 (**4**·3HCl), 999189 [**3**$(CuCN)_3$], 999190 [**3**$(CuCl)_3$], 999191 [**3**$(CuBr)_3$], 999192 [**3**$(CuCl_2)_3$], 999193 [**3**$(CuI_2)_3$], 999194 [**3**$(NiCl_2)_3$], 999195 [**3**$(AgCN)_3$], 999196 [**3**$(AgCl)_3$], 999197 [**3**$(AgBr)_3$], and 999198 [**3**$(AgI)_3$] contain the supplementary crystallographic data for this work.

■ AUTHOR INFORMATION

Corresponding Author

*Fax: +49-6221-545707. E-mail: hans-jorg.himmel@aci.uni-heidelberg.de.

Notes

The authors declare no competing financial interest.

■ ACKNOWLEDGMENTS

The authors gratefully acknowledge continuous financial support by the Deutsche Forschungsgemeinschaft (DFG).

■ REFERENCES

(1) Wettach, H.; Jester, S. S.; Colsmann, A.; Lemmer, U.; Rehmann, N.; Meerholz, K.; Höger, S. *Synth. Met.* **2010**, *160*, 691−700.

(2) Thiessen, A.; Wettach, H.; Meerholz, K.; Neese, F.; Höger, S.; Hertel, D. *Org. Electron.* **2012**, *13*, 71−83.

(3) Lang, N. D.; Solomon, P. M. *ACS Nano* **2009**, *3*, 1437−1440.

(4) Adam, D.; Schuhmacher, P.; Simmerer, J.; Häussling, L.; Siemensmeyer, K.; Etzbach, K. H.; Ringsdorf, H.; Haarer, D. *Nature* **1994**, *371*, 141−143.

(5) Gonell, S.; Poyatos, M.; Peris, E. *Angew. Chem., Int. Ed.* **2013**, *52*, 7009−7013.

(6) Li, K.; Xu, Z.; Xu, H.; Carroll, P. J.; Fettinger, J. C. *Inorg. Chem.* **2006**, *45*, 1032−1037.

(7) Huang, G.; Xu, H.; Zhou, X.-P.; Xu, Z.; Li, K.; Zeller, M.; Hunter, A. D. *Cryst. Growth Des.* **2007**, *7*, 2542−2547.

(8) (a) Hmadeh, M.; Lu, Z.; Liu, Z.; Gándara, F.; Furukawa, H.; Wan, S.; Augustyn, V.; Chang, R.; Liao, L.; Zhou, F.; Perre, E.; Ozolins, V.; Suenaga, K.; Duan, X.; Dunn, B.; Yamamto, Y.; Terasaki, O.; Yaghi, O. M. *Chem. Mater.* **2012**, *24*, 3511−3513. (b) Cui, J.; Xu, Z. *Chem. Commun.* **2014**, *50*, 3986−3988.

(9) (a) Edelmann, F. T. *Adv. Organomet. Chem.* **2008**, *57*, 183−352. (b) Edelmann, F. T. *Coord. Chem. Rev.* **1994**, *137*, 403−481. (c) Barker, J.; Kilner, M. *Coord. Chem. Rev.* **1994**, *133*, 219−300. (d) Bailey, P. J.; Price, S. *Coord. Chem. Rev.* **2001**, *214*, 91−141. (e) Herres-Pawlis, S. *Nachr. Chem.* **2009**, *57*, 20−23. (f) Coles, M. P. *Dalton Trans.* **2006**, 985−1001. (g) Coles, M. P. *Chem. Commun.* **2009**, 3659−3676. (h) Himmel, H.-J. In *Modeling of Molecular Properties*; Comba, P., Ed.; Wiley-VCH: Weinheim, Germany, 2011; Chapter 26, pp 425−453. (i) Jones, C. *Coord. Chem. Rev.* **2010**, *254*, 1273−1289. (j) Edelmann, F. T. *Adv. Organomet. Chem.* **2013**, *61*, 55−374.

(10) (a) Cotton, F. A.; Matonic, J. H.; Murillo, C. A. *J. Am. Chem. Soc.* **1997**, *119*, 7889−7890. (b) Bear, J. L.; Li, Y.; Han, B.; Kadish, K. M. *Inorg. Chem.* **1996**, *35*, 1395−1398. (c) Clérac, R.; Cotton, F. A.; Daniels, L. M.; Donahue, J. P.; Murillo, C. A.; Timmons, D. J. *Inorg. Chem.* **2000**, *39*, 2581−2584. (d) Cotton, F. A.; Murillo, C. A.; Wang, X.; Wilkinson, C. C. *Inorg. Chim. Acta* **2003**, *351*, 191−200.

(11) Day, B. M.; Mansfield, N. E.; Coles, M. P.; Hitchcock, P. B. *Chem. Commun.* **2011**, *47*, 4995−4997.
(12) (a) Green, S. P.; Jones, C.; Stasch, A. *Science* **2007**, *318*, 1754−1757. (b) Westerhausen, M. *Angew. Chem., Int. Ed.* **2008**, *47*, 2185−2187.
(13) (a) Börner, J.; Flörke, U.; Huber, K.; Döring, A.; Kuckling, D.; Herres-Pawlis, S. *Chem.−Eur. J.* **2009**, *15*, 2362−2376. (b) Börner, J.; dos Santos Vieira, I.; Pawlis, A.; Doering, A.; Kuckling, D.; Herres-Pawlis, S. *Chem.−Eur. J.* **2011**, *17*, 4507−4512. (c) Börner, J.; dos Santos Vieira, I.; Jones, M. D.; Döring, A.; Kuckling, D.; Flörke, U.; Herres-Pawlis, S. *Eur. J. Inorg. Chem.* **2011**, 4441−4456. (d) dos Santos Vieira, I.; Herres-Pawlis, S. *Eur. J. Inorg. Chem.* **2012**, 765−774. (e) dos Santos Vieira, I.; Herres-Pawlis, S. *Z. Naturforsch. B* **2012**, *67*, 320−330.
(14) (a) Würtele, C.; Gaoutchenova, E.; Harms, K.; Holthausen, M. C.; Sundermeyer, J.; Schindler, S. *Angew. Chem., Int. Ed.* **2006**, *45*, 3867−3869. (b) Maiti, D.; Lee, D.-H.; Gaoutchenova, K.; Würtele, C.; Holthausen, M. C.; Sarjeant, A. A. N.; Sundermeyer, J.; Schindler, S.; Karlin, K. D. *Angew. Chem., Int. Ed.* **2007**, *47*, 82−85. (c) Lanci, M. P.; Smirnov, V. V.; Cramer, C. J.; Gauchenova, E. V.; Sundermeyer, J.; Roth, J. P. *J. Am. Chem. Soc.* **2007**, *129*, 14697−14709. (d) Maiti, D.; Lee, D.-H.; Gaoutchenova, K.; Würtele, C.; Holthausen, M. C.; Sarjeant, A. A. N.; Sundermeyer, J.; Schindler, S.; Karlin, K. D. *Angew. Chem., Int. Ed.* **2008**, *47*, 82−85. (e) Peterson, R. L.; Ginsbach, J. W.; Cowley, R. E.; Qayyum, M. F.; Himes, R. A.; Siegler, M. A.; Moore, C. D.; Hedman, B.; Hodgson, K. O.; Fukuzumi, S.; Solomon, E. I.; Karlin, K. D. *J. Am. Chem. Soc.* **2013**, *135*, 16454−16467. (f) Saracini, C.; Liakos, D. G.; Zapata Rivera, J. E.; Neese, F.; Meyer, G. J.; Karlin, K. D. *J. Am. Chem. Soc.* **2014**, *136*, 1260−1263.
(15) Himmel, H.-J. *Z. Anorg. Allg. Chem.* **2013**, *639*, 1940−1952.
(16) Peters, A.; Kaifer, E.; Himmel, H.-J. *Eur. J. Org. Chem.* **2008**, 5907−5914.
(17) Peters, A.; Trumm, C.; Reinmuth, M.; Emeljanenko, D.; Kaifer, E.; Himmel, H.-J. *Eur. J. Inorg. Chem.* **2009**, 3791−3800.
(18) Trumm, C.; Hübner, O.; Kaifer, E.; Himmel, H.-J. *Eur. J. Inorg. Chem.* **2010**, 3102−3108.
(19) Emeljanenko, D.; Peters, A.; Wagner, N.; Beck, J.; Kaifer, E.; Himmel, H.-J. *Eur. J. Inorg. Chem.* **2010**, 1839−1846.
(20) Trumm, C.; Stang, S.; Eberle, B.; Kaifer, E.; Wagner, N.; Beck, J.; Bredow, T.; Meyerbröker, N.; Zharnikov, M.; Hübner, O.; Himmel, H.-J. *Eur. J. Inorg. Chem.* **2012**, 3156−3167.
(21) Emeljanenko, D.; Peters, A.; Vitske, V.; Kaifer, E.; Himmel, H.-J. *Eur. J. Inorg. Chem.* **2010**, 4783−4789.
(22) Stang, S.; Kaifer, E.; Himmel, H.-J. *Chem.−Eur. J.* **2014**, *20*, 5288−5297.
(23) Vitske, V.; Hermann, H.; Enders, M.; Kaifer, E.; Himmel, H.-J. *Chem.−Eur. J.* **2012**, *18*, 14108−14116.
(24) Herrmann, H.; Ziesak, A.; Wild, U.; Leingang, S.; Schrempp, D.; Wagner, N.; Beck, J.; Kaifer, E.; Wadepohl, H.; Himmel, H.-J. *ChemPhysChem* **2014**, 351−365.
(25) Peters, A.; Herrmann, H.; Magg, M.; Kaifer, E.; Himmel, H.-J. *Eur. J. Inorg. Chem.* **2012**, 1620−1631.
(26) Vitske, V.; König, C.; Kaifer, E.; Hübner, O.; Himmel, H.-J. *Eur. J. Inorg. Chem.* **2010**, 115−126.
(27) Kitagawa, S.; Masaoka, S. *Coord. Chem. Rev.* **2003**, *246*, 73−88.
(28) Patra, S.; Sarkar, B.; Ghumaan, S.; Fiedler, J.; Kaim, W.; Lahiri, G. K. *Dalton Trans.* **2004**, 754−758.
(29) Piglosiewicz, I. M.; Beckhaus, R.; Wittstock, G.; Saak, W.; Haase, D. *Inorg. Chem.* **2007**, *46*, 7610−7620.
(30) Herrera, J.-M.; Ward, M. D.; Adams, H.; Pope, S. J. A.; Faulkner, S. *Chem. Commun.* **2006**, 1851−1853.
(31) Klivansky, L. M.; Hanifi, D.; Koshkakaryan, G.; Holycross, D. R.; Gorski, E. K.; Wu, Q.; Chai, M.; Liu, Y. *Chem. Sci.* **2012**, *3*, 2009−2014.
(32) (a) Breslow, R.; Jaun, B.; Kluttz, R. Q.; Xia, C.-Z. *Tetrahedron* **1982**, *38*, 863−867. (b) Yatabe, T.; Harbison, M. A.; Brand, J. D.; Wagner, M.; Müllen, K.; Samori, P.; Rabe, J. P. *J. Mater. Chem.* **2000**, *10*, 1519−1525.
(33) Chen, L.; Kim, J.; Ishizuka, T.; Honsho, Y.; Saeki, A.; Seki, S.; Ihee, H.; Jiang, D. *J. Am. Chem. Soc.* **2009**, *131*, 7287−7292.
(34) Emeljanenko, D.; Peters, A.; Vitske, V.; Kaifer, E.; Himmel, H.-J. *Eur. J. Inorg. Chem.* **2010**, 4783−4789.
(35) Zacharias, P.; Gather, M. C.; Rojahn, M.; Nuyken, O.; Meerholz, K. *Angew. Chem., Int. Ed.* **2007**, *46*, 4388−4392.
(36) (a) Hopff, H.; Wick, A. K. *Helv. Chim. Acta* **1961**, *44*, 19−24. (b) Hopff, H.; Wick, A. K. *Helv. Chim. Acta* **1961**, *44*, 380−386. (c) Trætteberg, M.; Bakken, P.; Hopf, H.; Höpfner, T. *J. Mol. Struct.* **1998**, *445*, 99−105. (d) Iyoda, M.; Tanaka, S.; Otani, H.; Nose, M.; Oda, M. *J. Am. Chem. Soc.* **1988**, *110*, 8494−8500. (e) Stanger, A.; Ashkenazi, N.; Boese, R.; Bläser, D.; Stellberg, P. *Chem.−Eur. J.* **1997**, *3*, 208−211. (f) Shinozaki, S.; Hamura, T.; Ibusuki, Y.; Fujii, K.; Uekusa, H.; Suzuki, K. *Angew. Chem., Int. Ed.* **2010**, *49*, 3026−3029.
(37) Roquette, P.; Maronna, A.; Peters, A.; Kaifer, E.; Himmel, H.-J.; Hauf, Ch.; Herz, V.; Scheidt, E.-W.; Scherer, W. *Chem.−Eur. J.* **2010**, *16*, 1336−1350.
(38) Jesser, A.; Rohrmüller, M.; Schmidt, W. G.; Herres-Pawlis, S. *J. Comput. Chem.* **2014**, *35*, 1−17.
(39) Burdett, J. K.; Sevov, S. *J. Am. Chem. Soc.* **1995**, *117*, 12788−12792.
(40) Bowmaker, G. A.; Di Nicola, C.; Pettinari, C.; Skelton, B. W.; Somers, N.; White, A. H. *Dalton Trans.* **2011**, *40*, 5102−5115.
(41) Melzer, M. M.; Mossin, S.; Dai, X.; Bartell, A. M.; Kapoor, P.; Meyer, K.; Warren, T. H. *Angew. Chem., Int. Ed.* **2010**, *49*, 904−907.
(42) (a) Ryde, U.; Olsson, M. H. M.; Ross, B. O.; Borin, A. C. *Theor. Chem. Acc.* **2001**, *105*, 452−462. (b) Bryantsev, V. S.; Diallo, M. S.; Goodard, W. A., III. *J. Phys. Chem. A* **2009**, *113*, 9559−9567.
(43) Hoffmann, A.; Binder, S.; Jesser, A.; Haase, R.; Flörke, U.; Gnida, M.; Stagni, M. S.; Meyer-Klaucke, W.; Lebsanft, B.; Grünig, L. E.; Schneider, S.; Hashemi, M.; Goos, A.; Wetzel, A.; Rübhausen, M.; Herres-Pawlis. *Angew. Chem., Int. Ed.* **2014**, *53*, 299−304.
(44) Xiao, Z.; Donnelly, P. S.; Zimmermann, M.; Wedd, A. G. *Inorg. Chem.* **2008**, *47*, 4338−4347.
(45) Roquette, P.; Maronna, A.; Reinmuth, M.; Kaifer, E.; Enders, M.; Himmel, H.-J. *Inorg. Chem.* **2011**, *50*, 1942−1955.
(46) Maronna, A.; Hübner, O.; Enders, M.; Kaifer, E.; Himmel, H.-J. *Chem.−Eur. J.* **2013**, *19*, 8958−8977.
(47) Glaser, T.; Heidemeier, M.; Strautmann, J. B. H.; Bögge, H.; Stammler, A.; Krickemeyer, E.; Huenerbein, R.; Grimme, S.; Bothe, E.; Bill, E. *Chem.−Eur. J.* **2007**, *13*, 9191−9206.
(48) Bencini, A.; Gatteschi, D.; Totti, F.; McCleverty, J. A.; Ward, M. D. *J. Phys. Chem. A* **1998**, *102*, 10545−10551.
(49) (a) Roquette, P.; König, C.; Hübner, O.; Wagner, A.; Kaifer, E.; Enders, M.; Himmel, H.-J. *Eur. J. Inorg. Chem.* **2010**, 4770−4782. (b) Vitske, V.; Roquette, P.; Leingang, S.; Adam, C.; Kaifer, E.; Wadepohl, H.; Himmel, H.-J. *Eur. J. Inorg. Chem.* **2011**, 1593−1604.
(50) (a) Wolff, S. K.; Grimwood, D. J.; McKinnon, J. J.; Turner, M. J.; Jayatilaka, D.; Spackman, M. A. *CrystalExplorer 2.2*; University of Western Australia: Perth, Australia, 2010; available at http://hirshfeldsurface.net. (b) Turner, M. J.; McKinnon, J. J.; Jayatilaka, D.; Spackman, M. A. *CrystEngComm* **2011**, *13*, 1804−1813.
(51) Bill, E. *julX v.1.4.1—Simulation of Molecular Magnetic Data*; Max-Planck Institut for Bioinorganic Chemistry: Mülheim/Ruhr, Germany, 2008.
(52) *DENZO-SMN, Data Processing Software*; Nonius: Delft, The Netherlands, 1998; available at http://www.nonius.com.
(53) (a) Sheldrick, G. M. *SHELXS-97, Program for Crystal Structure Solution*; University of Göttingen: Göttingen, Germany, 1997; available at http://shelx.uni-ac.gwdg.de/SHELX/index.html. (b) Sheldrick, G. M. *SHELXL-97, Program for Crystal Structure Refinement*; University of Göttingen: Göttingen, Germany, 1997; available at http://shelx.uni-ac.gwdg.de/SHELX/index.html.
(54) *International Tables for X-ray Crystallography*; Kynoch Press: Birmingham, U.K., 1974; Vol. 4.
(55) (a) Spek, A. L. *J. Appl. Crystallogr.* **2003**, *36*, 7−13. (b) Spek, A. L. *PLATON, A Multipurpose Crystallographic Tool*; Utrecht University: Utrecht, The Netherlands, 2005.

(56) Zsolnai, L.; Huttner, G. *XPMA*; University of Heidelberg: Heidelberg, Germany, 1994; available at http://www.uni-heidelberg.de/institute/fak12/AC/huttner/soft-ware/software.html.
(57) Frisch, M. J.; Trucks, G. W.; Schlegel, H. B.; Scuseria, G. E.; Robb, M. A.; Cheeseman, J. R.; Scalmani, G.; Barone, V.; Mennucci, B.; Petersson, G. A.; Nakatsuji, H.; Caricato, M.; Li, X.; Hratchian, H. P.; Izmaylov, J. Bloino, A. F.; Zheng, G.; Sonnenberg, J. L.; Hada, M.; Ehara, M.; Toyota, K.; Fukuda, R.; Hasegawa, J.; Ishida, M.; Nakajima, T.; Honda, Y.; Kitao, O.; Nakai, H.; Vreven, T.; Montgomery, J. A., Jr.; Peralta, J. E.; Ogliaro, F.; Bearpark, M.; Heyd, E. Brothers, J. J.; Kudin, K. N.; Staroverov, V. N.; Kobayashi, R.; Normand, J.; Raghavachari, K.; Rendell, A.; Burant, J. C.; Iyengar, S. S.; Tomasi, J.; Cossi, M.; Rega, N.; Millam, J. M.; Klene, M.; Knox, J. E.; Cross, J. B.; Bakken, V.; Adamo, C.; Jaramillo, J.; Gomperts, R.; Stratmann, R. E.; Yazyev, O.; Austin, A. J.; Cammi, R.; Pomelli, C.; Ochterski, J. W.; Martin, R. L.; Morokuma, K.; Zakrzewski, V. G.; Voth, G. A.; Salvador, P.; Dannenberg, J. J.; Dapprich, S.; Daniels, A. D.; Farkas, O.; Foresman, J. B.; Ortiz, J. V.; Cioslowski, J.; Fox, D. J. *Gaussian 09*, Revision A.02; Gaussian Inc.: Wallingford, CT, 2009.
(58) (a) Ahlrichs, R.; Bär, M.; Häser, M.; Horn, H.; Kölmel, C. *Chem. Phys. Lett.* **1989**, *162*, 165−169. (b) Treutler, O.; Ahlrichs, R. *J. Chem. Phys.* **1995**, *102*, 346−354. (c) Eichkorn, K.; Treutler, O.; Öhm, H.; Häser, M.; Ahlrichs, R. *Chem. Phys. Lett.* **1995**, *242*, 652−660. (d) Sierka, M.; Hogekamp, A.; Ahlrichs, R. *J. Chem. Phys.* **2003**, *118*, 9136−9148. (e) Bauernschmitt, R.; Ahlrichs, R. *Chem. Phys. Lett.* **1996**, *256*, 454−464.
(59) (a) Stephens, P. J.; Devlin, F. J.; Chabalowski, C. F.; Frisch, M. J. *J. Chem. Phys.* **1994**, *98*, 11623−11627. (b) Becke, A. D. *J. Chem. Phys.* **1993**, *98*, 5648−5652. (c) Lee, C.; Yang, W.; Parr, R. G. *Phys. Rev. B* **1988**, *37*, 785−789.
(60) (a) Krishnan, R.; Binkley, J. S.; Seeger, R.; Pople, J. A. *J. Chem. Phys.* **1980**, *72*, 650−654. (b) McLean, A. D.; Chandler, G. S. *J. Chem. Phys.* **1980**, *72*, 5639−5648.
(61) Weigend, F.; Ahlrichs, R. *Phys. Chem. Chem. Chem. Phys.* **2005**, *7*, 3297−3305.
(62) Weigend, F. *Phys. Chem. Chem. Chem. Phys.* **2006**, *8*, 1057−1065.